

Article

# Monitoring Single-Phase LV Charging of Electric Vehicles

Piotr Kuwałek , Grzegorz Wiczyński \* 

Institute of Electrical Engineering and Electronics, Poznan University of Technology, Piotrowo Street, No. 3a, 60-965 Poznan, Poland

\* Correspondence: grzegorz.wiczynski@put.poznan.pl

**Abstract:** The paper presents the results of the monitoring process of the charging of an electric vehicle battery pack. Battery pack charging with a capacity of 58 kWh was monitored in a single-phase 230 V/50 Hz circuit. The slow charging system used was configured to obtain a current of 10 A. During monitoring, the focus was on the recognition of the charging, considering the impact of this process on power quality and, consequently, on the reliability of electrical machines. Research results show that the monitored charges are one-, two-, or three-stage processes. The variations in the currents, power, and higher harmonic contents were observed. The effects of such variations depend on the properties of the power grid at the point of connection of the charging system. Knowledge of the variation of the voltages, currents, and active and reactive power allows for the determination of the requirements of the measuring equipment used for charging the monitoring, including the selection of discrimination/averaging time of monitored quantities. The research results also indicate the need for continuous monitoring of the power quality in the power supply circuit of electrical loads, e.g., electrical machines. Continuous monitoring supports the diagnostics of electrical machines and allows the appropriate measures to increase their reliability.

**Keywords:** charging process; electric vehicles; power quality monitoring; reliability of electrical machines



**Citation:** Kuwałek, P.; Wiczyński, G. Monitoring Single-Phase LV Charging of Electric Vehicles. *Sensors* **2023**, *23*, 141. <https://doi.org/10.3390/s23010141>

Academic Editor: Martin Riera-Guasp

Received: 19 November 2022

Revised: 17 December 2022

Accepted: 19 December 2022

Published: 23 December 2022



**Copyright:** © 2022 by the authors. Licensee MDPI, Basel, Switzerland. This article is an open access article distributed under the terms and conditions of the Creative Commons Attribution (CC BY) license (<https://creativecommons.org/licenses/by/4.0/>).

## 1. Introduction

In the power grid, multiple disturbances of power quality are common, such as voltage distortion caused by higher harmonics, voltage asymmetry, and voltage fluctuations [1]. Disturbances in the power quality have negative impacts on particular elements of the power system, including electric machines [2,3], causing, e.g., their overheating [4], excessive vibrations [5], torsional vibrations [6], reduced efficiency [7], loss of reliability, and durability [8–10]. Power quality disturbances that occur in the power grid and affect the reliability of electrical machines include, among others, voltage fluctuations [11,12], voltage distortions caused by higher harmonics [13] or inter-harmonics [14,15]. At the same time, in some cases, the operation of electric machines or devices associated with them can also cause disturbances of power quality [16–18], for example, the electric machine control or the charging of an electric vehicle (EV) [19,20]. The consequence of the appearance of the reduced power quality is the reduction of the reliability of other loads (including electric machines) supplied from the same power grid. Therefore, it is necessary to continuously monitor the parameters determining the power quality [21] to identify early the occurrence of disturbances of power quality and take appropriate actions (e.g., activation of active parallel filters [22–24], activation of the voltage stabilizers [25,26], and activation of intelligent correction systems of the quality level of the supply voltage [27,28]) to reduce the potential effects of disturbances of power quality. Therefore, monitoring the parameters of the supply voltage [29] for individual power loads (including electrical machines) contributes to increasing their reliability.

In recent years, there has been a significant increase in interest in electric vehicles. In response to this trend, appropriate actions are taken to adapt the power infrastructure (e.g., fast charging stations for electric vehicles are installed in power grids). Electric vehicles can

also be charged in households using appropriately adapted single-phase chargers. This method of the charging has become popular in recent years due to the convenience of use and economic aspects [30]. At the same time, this method of the charging is the worst from the point of view of power quality, due to the low short-circuit power in low-voltage power grids, especially in the cases of the charging of electric vehicles in households located at a considerable distance from the power station (consumers at the end of the line in the radial topology of low-voltage (LV) networks). In such situations, there are increased phenomena that reduce the power quality and, as a consequence, have negative impacts on other power loads, which are supplied from the same power grids where electric vehicles are charged. In recent years, many problems caused by the charging of electric vehicles have been identified, e.g., voltage distortion caused by higher harmonics [31–34], voltage variation caused by the dynamics of electric vehicle charging processes [35–38], and the generation of supraharmonics caused by the power electronics of electric vehicle chargers [39,40]. It is worth noting that in the indicated research results, an attempt is made to generalize, joining certain types of electric vehicle chargers with specific power quality disturbances, which are strictly defined in their nature. On this basis, many methods of evaluation and counteraction of interference caused by electric vehicle chargers are defined [41–44]. However, in the real power grid, there is a mutual interaction between the current forced by the electric vehicle chargers, which affects the process of the charging of batteries of electric vehicles and the quality of the supply voltage. Such a state may hinder the actions aimed at minimizing disturbances caused by electric vehicle chargers. Therefore, it is necessary to continuously study and monitor the variations of processes during the charging of electric vehicles, so that solutions that improve power quality are effective [45,46].

The paper presents the selected results of monitoring the charging process of an electric vehicle from the single-phase low-voltage (LV) network. During the monitoring, the non-stationarity of the charging process is observed, within which it is possible to indicate a different number of stages, which (to a certain extent and in different ways) affect the reduction of power quality. The long-term results of the observations indicate that even for one specific type of EV onboard charger supplied from the same supply circuit (the supply circuit with the high short-circuit power in the LV network), different natures of EV charger processes are observed each time, characterized by different changes in parameters determining the power quality. The presented research results indicate the need for continuous monitoring of the quality of the supply voltage for electric machines, especially when the electric vehicle is charged in the same supply circuit because the effects of the impacts during vehicle charging can be difficult to predict due to the non-stationarity of this process. Unusual cases are also presented, in which the relationship between the individual harmonics of the EV charger current and its supply voltage is notable (the strong potential impact of the EV charger on the supply voltage despite the low impedance of the supply circuit). Section 2 presents the research object and discusses research conditions. Section 3 presents and discusses the obtained measurement results. Section 4 presents the final conclusions resulting from the presented selected results of the research carried out.

## 2. Materials and Methods

The research object involved charging the battery pack of an electric vehicle from the side of the power grid. The charging process was monitored in a three-phase 230 V/50 Hz low-voltage (LV) network. The public buildings were also supplied from the same supply circuit to which the charger was connected. There were different loads in public buildings that affected the supply voltage. The battery pack was charged in a single-phase circuit. The length of the power line (from the MV/LV transformer to the supply point of the charging system, where MV is the medium voltage) is short. Thus, the impedance of the power supply circuit was low, and the impact of the charging system on the power grid was negligible. The diagram of the power supply circuit of the tested battery pack charging system is shown in Figure 1.

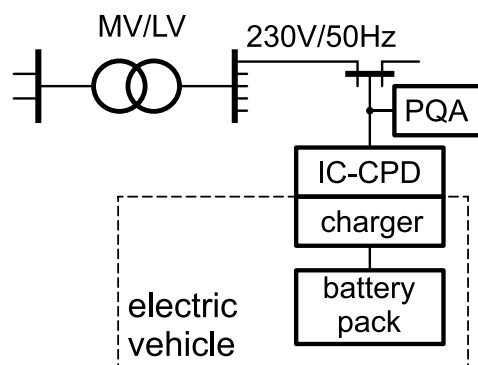


**Figure 1.** The diagram of the battery pack charging circuit with the measurement point marked, where MV/LV is the medium-voltage to low-voltage transformer, PQA is the power quality analyzer, IC-CPD is the in-cable control and protection device, and the charger is the battery pack charging process control system.

The battery pack is a set of 216 lithium-ion cells with a nominal voltage of 3.65 V and a capacity of 78 Ah. The total capacity of the pack is 62 kWh with a usable capacity of 58 kWh (94%). The IC-CPD system with a 230 V/50 Hz power grid is configured to consume 10 A of the current (mode 2 [47]). During charging, the IC-CPD system was supplied with a non-stabilized voltage (changed according to the voltage on the MV side and the power consumption of loads, which are supplied from the same supply circuit). There is no detailed information about the charger. Despite attempts to obtain technical documentation for the tested charger, the manufacturer refused to provide detailed technical information, citing the confidential data clause. Figure 2 shows a photo of an electric vehicle whose charging process was monitored.



**Figure 2.** The photo of the connector in electric vehicle (during charging) and the charging current controller (IC-CPD).

The process of charging an electric vehicle, as indicated in Figure 2, was monitored from May to November 2022. During the monitoring, parameters determining power quality [48] were recorded: fundamental voltage frequency, rms value of the voltage  $U$  and current  $I$ , active  $P$  and reactive  $Q$  power, active  $E_P$  and reactive  $E_Q$  energy, higher harmonics of the voltage  $u_h$  and current  $i_h$ , total harmonic distortion (THD) factor of the voltage THDU and current THDI, short-term  $P_{st}$  and long-term  $P_{lt}$  flicker indicator, asymmetry coefficients, voltage fluctuation indices, with the use of the SPE energy power quality analyzer [49]. The indicated parameters (maximum, average, and minimum values) were recorded in intervals from 10 s to 60 s, except for the indicator  $P_{st}$ , which was recorded with an interval of 10 min. The measurement uncertainty of:

- rms value of the voltage  $U$ :  $\pm 0.1\% U_{din}$ , where the declared input voltage  $U_{din} = 230$  V;
- indicator  $P_{st}$ : 0.05 for  $P_{st} \leq 1$  and  $5\% P_{stm}$  for  $P_{st} > 1$ , where  $P_{stm}$  is the measurement result;
- individual harmonics:  $0.05\% U_{din}$  for  $U_h < 0.01 U_{din}$  and  $5\% U_h$  for  $U_h \geq 0.01 U_{din}$ ;
- Total Harmonic Distortion (THD) factor of the voltage THDU and current THDI: 0.05%;
- rms value of the current  $I$ :  $\pm 0.1\% I_{range}$ , where the current range  $I_{range} = 30$  A;
- active power:  $\pm 0.15\% (U_{din} \cdot I_{range})$ ;

- reactive power (according to Budeanu's concept):  $\pm 0.2\% (U_{\text{din}} \cdot I_{\text{range}})$ .

Phase voltages were measured directly. The current clamp Kyoritsu KEW8146 [50] was used to measure the EV charger current (rated current: 30 A; output voltage: 50 mV/A; measurement uncertainty in the range 0–15 A:  $\pm 1.0\%$  of reading (50/60 Hz) and  $\pm 2.0\%$  of reading (40 Hz–1 kHz); dimensions: 100 × 60 × 26 mm; max. conductor diameter: 24 mm). The measurement inaccuracies of parameters determining the power quality by the used power quality analyzer were at the levels specified by the standard IEC 61000-4-30 [51]. The monitoring of the indicated parameters was carried out during the charging of the electric vehicle, as well as when the electric vehicle was not being charged, to know the nature of power loads, which were supplied from the same supply circuit as the electric vehicle charger. Such actions carried out in the long-term make it possible to minimize the probability of incorrect conclusions about the impact of the EV onboard charger on the power quality. Each time, the EV charging process ended with 80% of the battery charge according to the algorithm set in the EV onboard charger control system. During measurements, information about changes in the actual state of the charge of the battery was not recorded.

The paper presents five selected examples of battery pack charging for different discharge states. Table 1 summarizes information on active and reactive energy supplied during the charging process. Selected examples are characterized by different numbers of stages with different numbers of sub-stages that were observed during the charging process. The  $X$ -th stage (stage  $X_i$ ) is understood as a state in which the nature of capacitive reactive power consumed by the system is quasi-stationary. Thus, a step change regarding the reactive power consumed results in the separation of the next stage. In turn, a step change in the nature of the active power variation associated with a step change in at least one other selected recorded parameter results in the separation of the  $i$ -th sub-stage of the  $X$ -th stage (stage  $X_i$ ). The other recorded parameters were, e.g., the minimum  $P_{\text{min}}$ , average  $P_{\text{avg}}$ , and maximum  $P_{\text{max}}$  values of active power, the THDU factor of supply voltage, the THDI factor of consumed current, and individual  $h$ -th higher harmonics of the current  $i_h$ , and voltage  $u_h$ .

**Table 1.** Summary of the selected charging processes.

| Case No. | $E_P$ [kWh] | $E_Q$ [kvarh] | $T_{\text{charge}}$ [min] | $T_{\text{REC}}$ [s] | Remarks   |
|----------|-------------|---------------|---------------------------|----------------------|---|
| I        | 3.9         | 0.6 lead      | 104                       | 30                   | Main charging phase consisting of 2 stages (2 sub-stages in stage 2)  |
| II       | 6.1         | 1.2 lead      | 164                       | 10                   | Main charging phase consisting of 2 stages (2 sub-stages in stage 2)  |
| III      | 25.5        | 4.7 lead      | 674                       | 10                   | Main charging phase consisting of 2 stages (2 sub-stages in stage 2) and additional charging phase consisting of 2 stages |
| IV       | 33.7        | 6.8 lead      | 884                       | 20                   | Main charging phase consisting of one stage and two additional phases consisting of two and one stage respectively        |
| V        | 36.7        | 6.8 lead      | 982                       | 10                   | Main charging phase consisting of 3 stages (3 sub-stages in stage 2)  |

The battery pack charging process is performed in the constant current (CC) or the constant voltage (CV) mode [52–54]. The charging process starts in CC mode. For this mode of the charging process, a slow increase in the charging power can occur due to a slow increase of the voltage on the battery pack and it cannot cause short-term changes in the current and power of the EV onboard charger. Moreover, the CV mode does not cause rapid changes in power consumption. It should be noted that such EV onboard chargers

are power electronic systems with built-in regulators [55,56]. For example, a power factor compensation (PFC) [54,57] is commonly built in. Such a system includes a regulator whose task is to obtain a power factor  $\cos \varphi$  with a value close to 1. The operation of regulators, for example, in interaction with changes in the supply voltage [57–59], can cause additional changes in the power consumed by EV onboard chargers, in proportion to the control algorithm used.

### 3. Results and Discussion

#### 3.1. Case I

The charging system was supplied with non-stabilized voltage from the LV power grid during the monitoring, as mentioned in Section 2. In the monitoring process, the supply voltage values are changing, as shown in Figure 3. The variations of RMS values of the voltages are shown in the characteristics  $U_{\max} = f(t)$ ,  $U_{\text{avg}} = f(t)$  and  $U_{\min} = f(t)$  (where:  $U_{\max}$ ,  $U_{\text{avg}}$  and  $U_{\min}$  are, respectively, the maximum, average, and minimum rms values determined for the interval  $T_{\text{REC}} = 30$  s) along with the characteristic  $P_{st} = f(t)$ . Figure 3 also shows the characteristics of maximum  $I_{\max} = f(t)$  and minimum  $I_{\min} = f(t)$  values of rms values of the current.

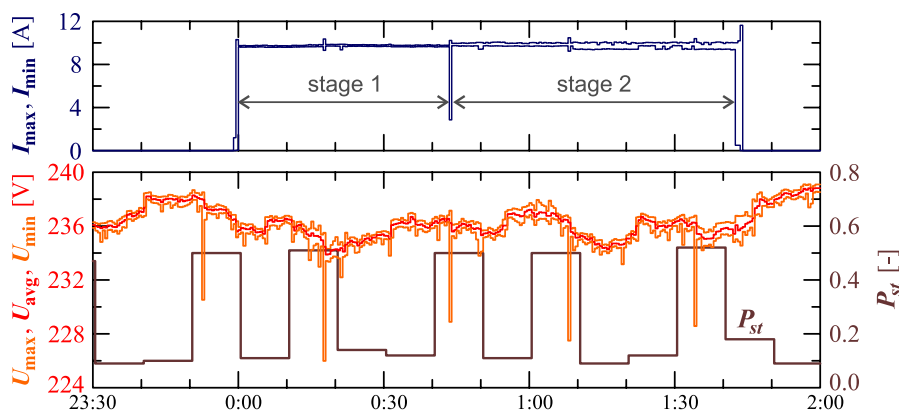


**Figure 3.** The characteristics of maximum  $U_{\max} = f(t)$ , average  $U_{\text{avg}} = f(t)$  and minimum  $U_{\min} = f(t)$  values of rms values of supply voltage and characteristic  $P_{st} = f(t)$  for Case I.

Figure 3 shows slow voltage changes (in the range of  $\pm 6$  V) with short-term decreases every 27 min. By monitoring voltage variations in a weekly time horizon (during charging and beyond), it was found that short-term voltage decreases are caused by the cyclical operation of a disturbing load active for some part of the day. It should be emphasized that rms values of the voltages meet the normative requirements of standard EN 50160 [48], i.e., rms values of the voltages are in the range of  $230 \text{ V} \pm 10\%$ . Moreover, voltage fluctuations, expressed by the short-term flicker indicator  $P_{st}$ , meet the normative requirements of the standard EN 50160 [48] ( $P_{st} \leq 1$ ).

Figure 4 shows the maximum  $P_{\max}$  and minimum  $P_{\min}$  characteristics of active power and average reactive power  $Q_{\text{avg}}$  during active charging for 104 min.

Regarding the characteristics of reactive power (Figure 4), two stages can be easily indicated. In addition, there are 2 sub-stages in stage 2 (stage 2a and stage 2b).

Figure 5 shows the characteristics of maximum  $P_{\max}$ , average  $P_{\text{avg}}$  and minimum  $P_{\min}$  values of active power (on a properly scaled characteristic).

The characteristics of Figure 5 in stage I show a slow linear increase in the active power consumed. This can indicate that the battery pack is charging in a constant current mode. In stage 2 (at stage 2a and stage 2b), the charging mode changes while the increases in active power change. Short-term undervoltages cause short-term increases in active power changes. However, due to the short duration of this phenomenon, it does not have a significant impact on the charging process.

Figure 6 shows the difference between the maximum  $P_{\max}$  and minimum  $P_{\min}$  active power determined for the interval  $T_{\text{REC}} = 30$  s.

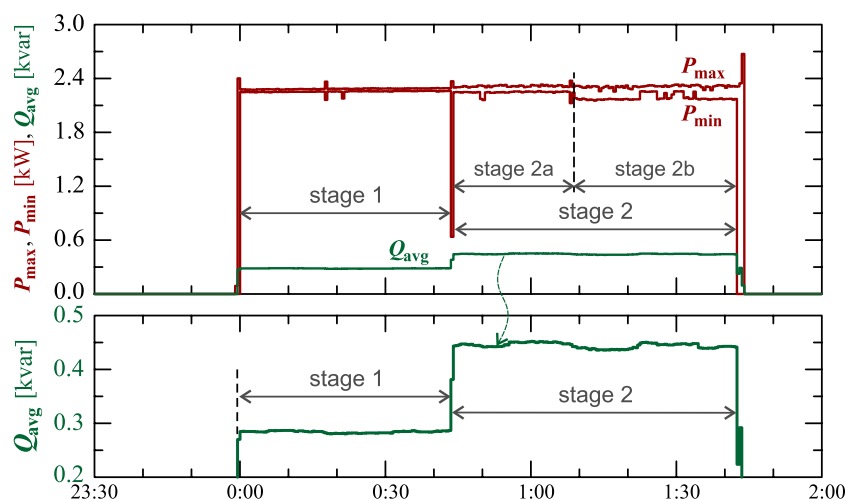


**Figure 4.** The characteristics of maximum  $P_{\max} = f(t)$  and minimum  $P_{\min} = f(t)$  values of active power and average values of reactive power  $Q_{\text{avg}} = f(t)$  for Case I.

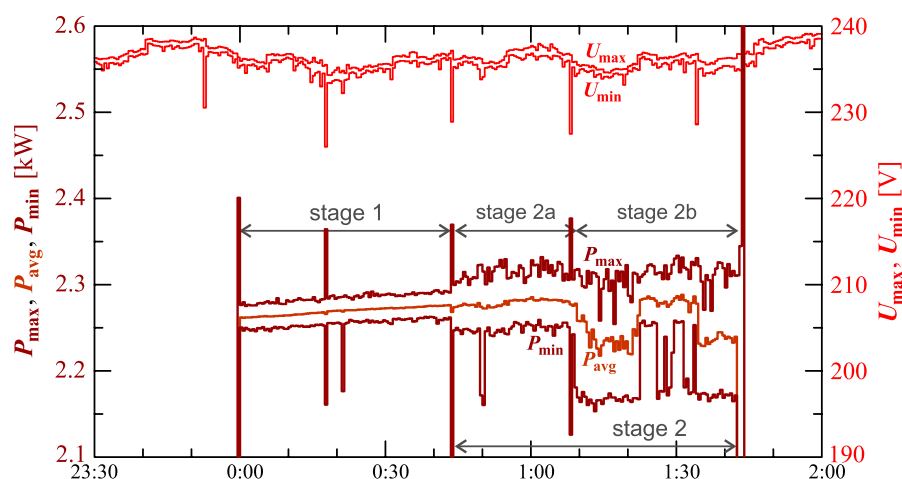


**Figure 5.** The characteristics of maximum  $P_{\max} = f(t)$ , average  $P_{\text{avg}} = f(t)$ , and minimum  $P_{\min} = f(t)$  values of active power and maximum  $U_{\max} = f(t)$  and minimum  $U_{\min} = f(t)$  rms values of the supply voltage for Case I.

The characteristic in Figure 6 clearly shows the increase in active power changes ( $P_{\max} - P_{\min}$ ) in successive stages. In stage 1, the variation is approximately 30 W, in stage 2b, it increases to approximately 150 W.

The indicated stages of the charging process are determined by analyzing the nature of the active and reactive power. However, stages/sub-stages of the charging process can be determined by analyzing the current and voltage harmonics. Figure 6 also shows the characteristics of the current and voltage THD factors. Comparing the characteristics of the current and voltage THD factors, it can be noticed that there is no dependency between the changes in the current and voltage distortions (i.e., the increase in the current distortion is not caused by the increase in the voltage distortion). The current THD factor suggests the division of the charging process into two stages. In stage 1, the nature of the current and voltage THD factors are similar. In stage 2, the values of the current THD factor increase while the values of the voltage THD factor is kept (approximately) constant.

Information about the charging process can be provided by analyzing individual higher harmonics. Considering the properties of discrete Fourier transform (DFT), even harmonics can be expected in the case of power variation (thus, current variations). Figure 7 shows characteristics of the voltage and current THD factors and the characteristics of the second harmonics of the current and voltage.

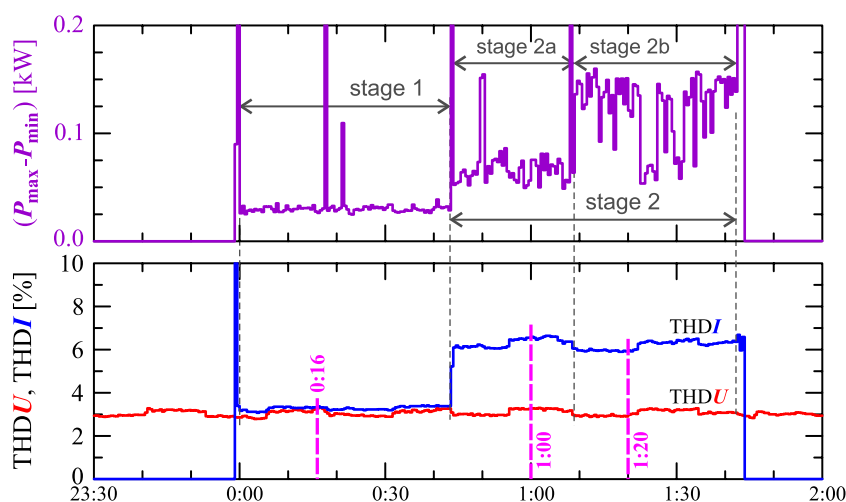


**Figure 6.** The differences between the maximum and minimum active power  $(P_{\max} - P_{\min}) = f(t)$  (top), and the voltage THD factor  $\text{THDU} = f(t)$  and current THD factor  $\text{THDI} = f(t)$  (bottom) with the marking of measurement results presented on the waveforms (Figure 11) and amplitude spectra (Figure 10) recorded at 0:16, 1:00, and 1:20 for Case I.

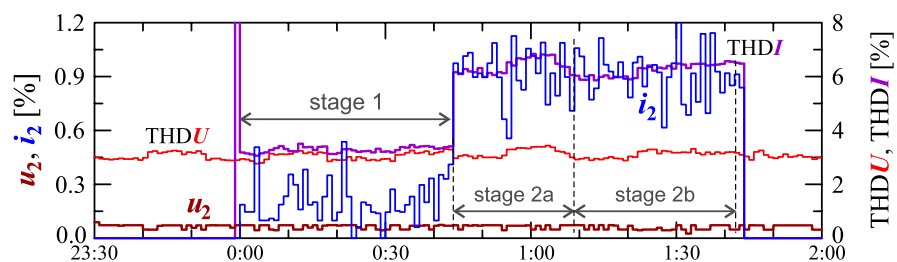


**Figure 7.** The characteristics of the voltage THD factor  $\text{THDU} = f(t)$  and the current THD factor  $\text{THDI} = f(t)$  and the characteristics of the second harmonics of the current  $i_2 = f(t)$  and voltage  $u_2 = f(t)$  for Case I.

As expected, the occurrence of the second harmonic of the current is correlated with the occurrence of the current variation. The characteristic of this harmonic, similar to the characteristic of the current THD factor, suggests the division of the charging process into two stages. Information about the charging process can be obtained by analyzing higher harmonics.

The characteristics of odd harmonics of the current  $i_h$  from the order  $h = 3$  to 19 are shown in Figure 8. Analyzing Figure 8, an analogous trend for the 2nd order harmonic can be seen, similar to the odd harmonics from the 3rd to the 13th order when charging an electric vehicle. For the 5th harmonic, there is the same strong correlation with the current THD factor as for the 2nd harmonic. In stage 1, after the start of the charging, the individual harmonics first increase to a quasi-determined level. In stage 2, during vehicle charging, when the power variation increases, subsequent increases in the values of individual harmonics are observed. Moreover, individual sub-stages (stage 2a and stage 2b) can be observed in the case of characteristics of the 5th-, 7th-, 11th-, and 13th-order harmonics. The indicated harmonics in stage 2 are periodically monotonic, one sub-stage (stage 2a/stage 2b) has a period of increase and a period of decrease in the value of individual harmonics. The indicated harmonics in stage 2 are probably related to the increase in the impact of the power electronic converter in the charging system, which is associated with the harmonics of the order of  $6n \pm 1$ , where  $n$  is any natural number. During charging an electric vehicle, there are also harmonics in the current higher orders than harmonics presented in Figure 8. This can be seen in Figure 9. Analyzing Figure 9, it can be seen that during the charging of an electric vehicle, the contribution of higher harmonics from the order of 15 is also revealed. In the case of these harmonics, there is no visible change in their nature in individual stages and sub-stages. During the entire

charging process, harmonics higher than the 15th order fluctuate around one quasi-definite level, the value of which is different for individual harmonics. The occurrence of higher harmonics indicates that the signal is distorted.

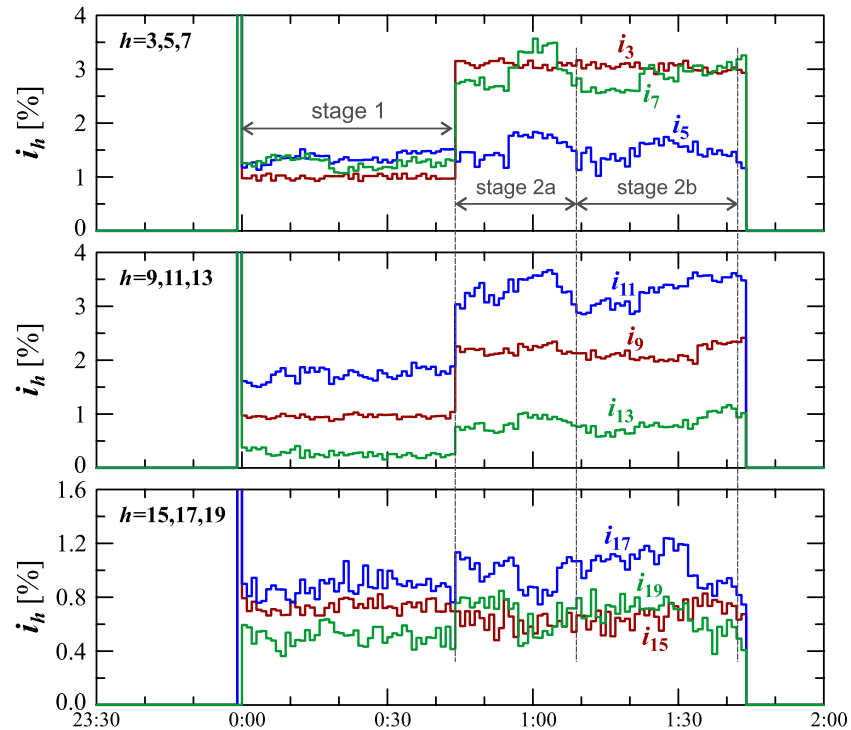


**Figure 8.** The characteristics of odd harmonics of the current  $i_h = f(t)$  from the order  $h = 3$  to 19 for Case I.

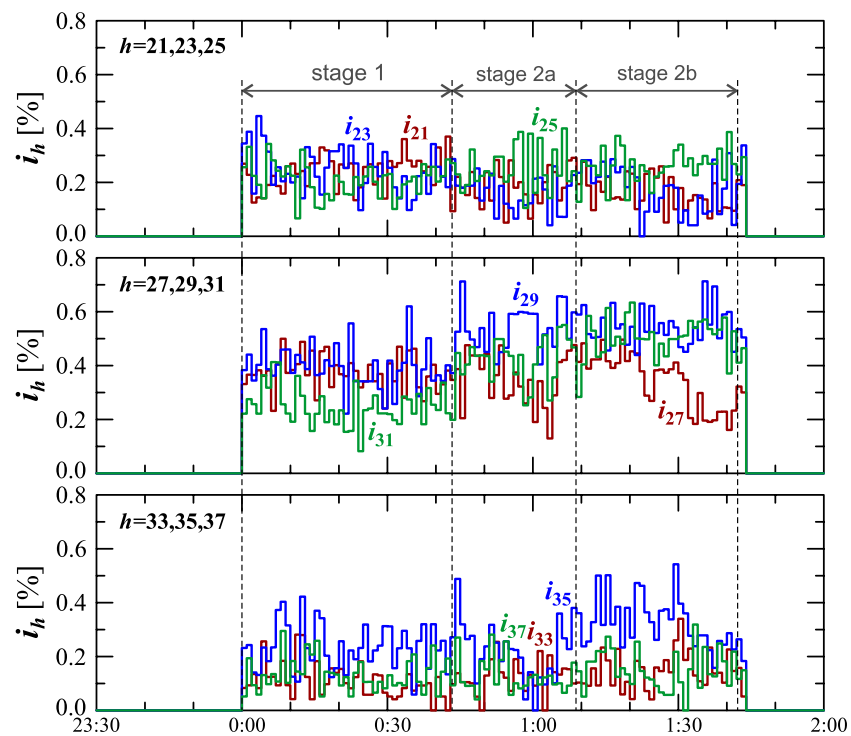


**Figure 9.** The characteristics of odd harmonics of the current  $i_h = f(t)$  from the order  $h = 21$  to 37 for Case I.

Figure 10 shows the amplitude spectrum of the current recorded at 00:16, 1:00, and 1:20 (recording times are marked in Figure 6). Recreated current waveforms on the basis of recorded harmonics are shown in Figure 11.

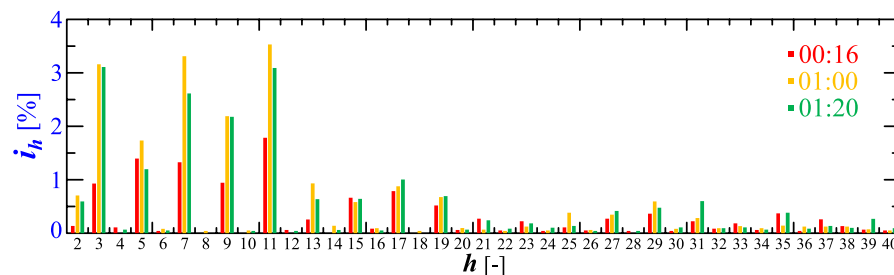


Figure 10. The amplitude spectrum of the current  $i_h = f(h)$  recorded at 00:16, 1:00, and 1:20 for Case I.

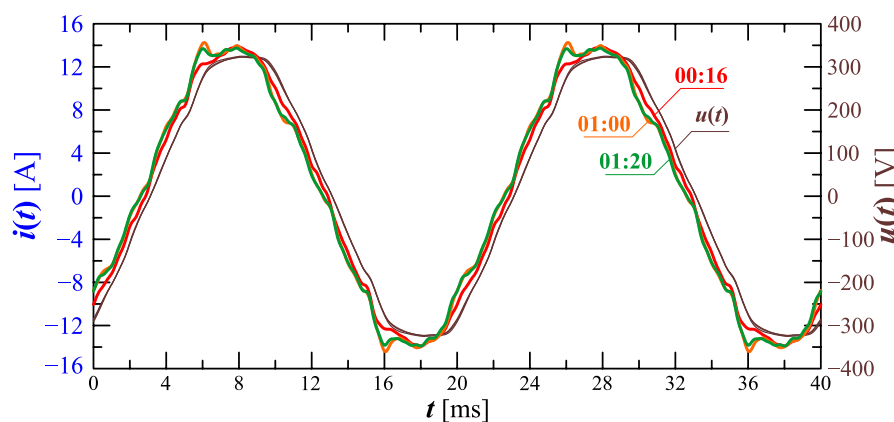


Figure 11. Recreated voltage waveforms  $u(t)$  and current waveforms  $i(t)$  recorded at 00:16, 1:00, and 1:20 for Case I.

Analyzing characteristics of the current THD factor in Figures 6 and 7, it can be seen that in the initial charging phase (approximately 00:00) the deformation increases. The start of the charging is depicted in Figures 12 and 13 showing the amplitude spectrum and current waveforms at 00:00, 00:01, and 00:02.

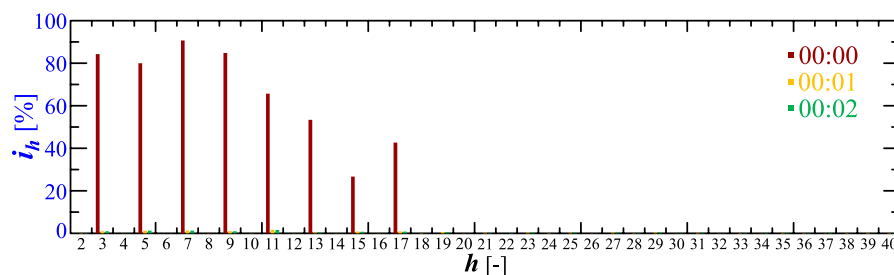
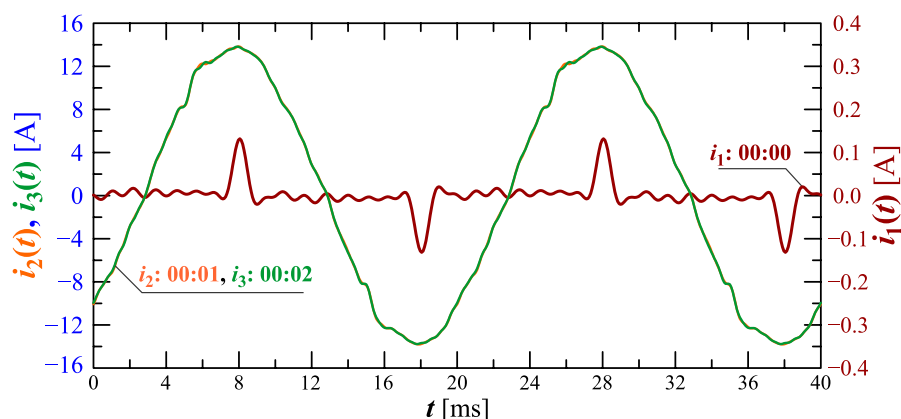


Figure 12. The amplitude spectrum of the current  $i_h = f(h)$  recorded at 00:00, 00:01, and 00:02 for Case I.

Analyzing characteristics from Figures 10–13, one can notice a significant non-stationarity of the charging process, characterized by current waveform changes, and, thus, the changes in the contribution of individual harmonic values, in subsequent time steps. Based on the waveforms presented in Figures 11 and 13, conclusions can also be made regarding the requirements of measurement equipment used to measure selected quantities during the charging of an electric vehicle. Namely, it is worth noting that the current waveform is strongly non-stationary in time, and as a consequence, it can lead to significant errors in the measurement of higher harmonics (e.g., by carrying out the measurement in accordance with the requirements of standard IEC 61000-4-30 [51] referring to the standard

IEC 61000-4-7 [60] for harmonics measurement) due to the phenomenon of “spectrum leakage” [61]. In such situations, considering quasi-periodic states (such as those presented in Figures 11 and 13), it is necessary to detect fundamental periods using advanced signal processing methods (e.g., using the ESPRIT method [62]). Only after the effective detection of indicated quasi-fundamental periods is it possible to correctly determine all parameters calculated for the periodic waveforms (rms values of higher harmonics, THD factor, rms value of signal, active and reactive power). It is also worth noting the shapes of the separated quasi-periods of the current waveforms in time. For this type of waveform, the value of the crest factor is much more different from  $\sqrt{2}$  (see Figure 13), so the use of equipment based on a crest detector also leads to significant errors in the measurement of the rms value of the current during the charging of an electric vehicle. On the other hand, in the case of the measurement equipment that allows the true rms to be determined, the aspect of the appropriate selection of the fundamental period occurs.



**Figure 13.** Recreated voltage waveforms  $u(t)$  and current waveforms  $i(t)$  recorded at 00:00, 00:01, and 00:02 for Case I.

### 3.2. Case II

During the charging process defined as Case II, as in Case I, the supply voltage changes, as shown in Figure 14. The variation of rms voltage values is shown in the characteristics  $U_{\max} = f(t)$ ,  $U_{\text{avg}} = f(t)$  and  $U_{\min} = f(t)$  (where:  $U_{\max}$ ,  $U_{\text{avg}}$  and  $U_{\min}$  are respectively the maximum, average, and minimum rms values determined for the interval  $T_{\text{REC}} = 10$  s) along with the characteristic  $P_{st} = f(t)$ . Figure 14 also shows the characteristics of maximum  $I_{\max} = f(t)$  and minimum  $I_{\min} = f(t)$  values of rms values of the current.

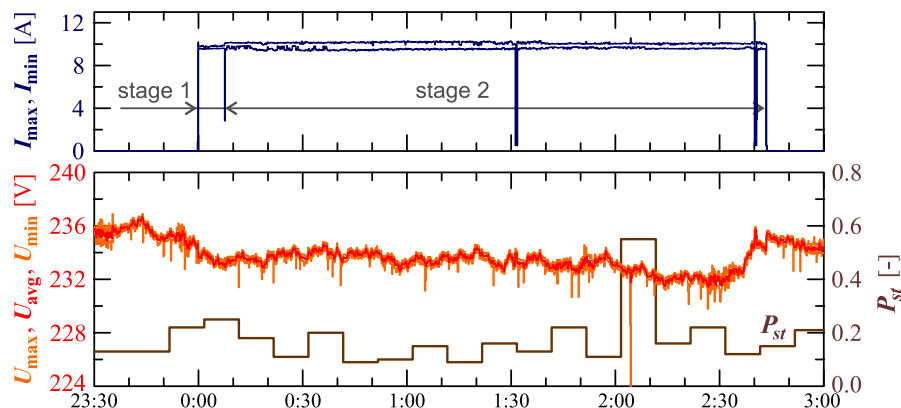


**Figure 14.** The characteristics of maximum  $U_{\max} = f(t)$ , average  $U_{\text{avg}} = f(t)$ , and minimum  $U_{\min} = f(t)$  values of rms values of the supply voltage and characteristic  $P_{st} = f(t)$  for Case II.

Figure 14 shows slow voltage changes (typically in the  $\pm 4\text{ V}$  range) with short-term decreases every few minutes. As in Case I, the observed voltage variation in a weekly time horizon (during charging and beyond) indicates that short-term undervoltages are caused by the cyclical operation of a disturbing load active for part of the day, unrelated to the tested vehicle charging system. It should be emphasized that the rms values of the voltage are in the range of  $230\text{ V} \pm 10\%$ . Voltage fluctuations expressed by the short-term flicker indicator  $P_{st}$ , as in Case I, meet the normative requirements of standard EN 50160 [48] ( $P_{st} \leq 1$ ).

Figure 15 shows the characteristics of the maximum  $P_{max}$  and minimum  $P_{min}$  of the active power and average reactive power  $Q_{avg}$  during the active charging for 164 min. Analyzing the characteristics of the reactive power (Figure 15), two stages can be identified, but in stage 2, two sub-stages can be separated (stage 2a and stage 2b).

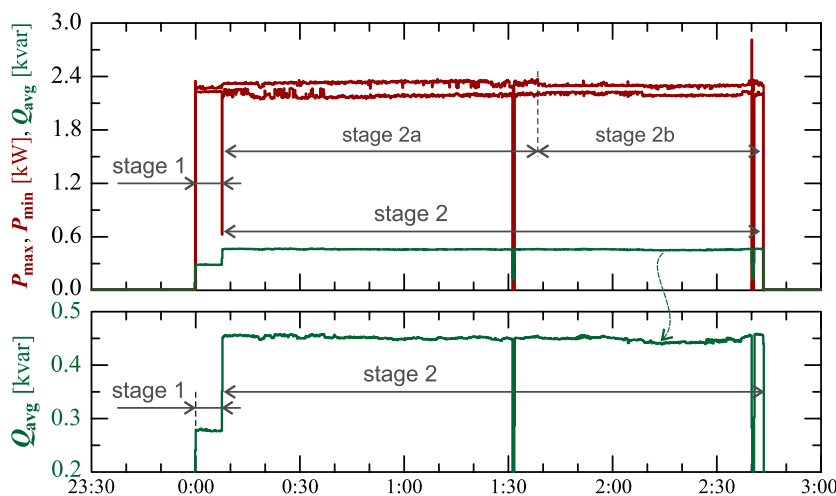


Figure 15. The characteristics of the maximum  $P_{max} = f(t)$  and minimum  $P_{min} = f(t)$  values of active power and average values of reactive power  $Q_{avg} = f(t)$  for Case II.

Figure 16 shows the characteristics of the maximum  $P_{max}$ , average  $P_{avg}$ , and minimum  $P_{min}$  of the active power, on a properly scaled characteristic, in relation to the characteristics of maximum  $U_{max}$  and minimum  $U_{min}$  rms values of the voltage, to better highlight the active power changes during the charging of an electric vehicle.

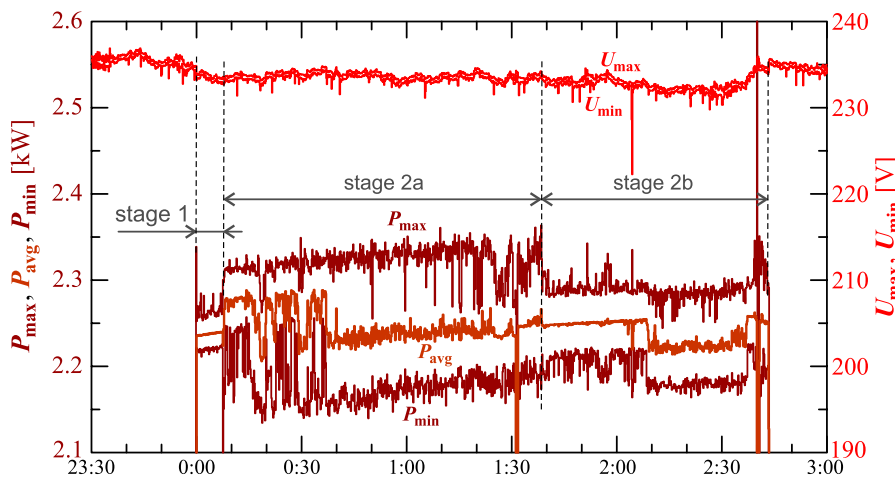
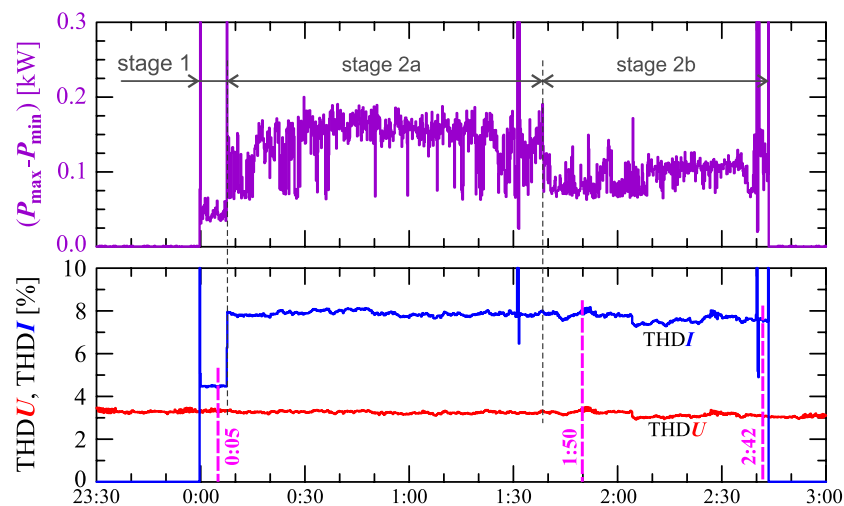


Figure 16. The characteristic of the maximum  $P_{max} = f(t)$ , average  $P_{avg} = f(t)$ , and minimum  $P_{min} = f(t)$  values of the active power and maximum  $U_{max} = f(t)$  and minimum  $U_{min} = f(t)$  rms values of the supply voltage for Case II.

In stage 1 of characteristic in Figure 16, a slow linear increase of average values of active power can be seen. In stage 2a the nature of the charging process changes. Stage 2a starts with a step increase in average values of active power. At the same time, there is an increase in active power changes. In stage 2, there is a trend of increasing active power associated with several step changes in the average values of active power. In stage 2b, there is a reduction in active power changes compared to stage 2a. Short-term undervoltages cause short-term increases in power active changes. However, due to the short duration of this phenomenon, it does not have a significant impact on the charging process. It should be noted that the largest active power changes (Figures 14–16) are not correlated with undervoltages.

Figure 17 shows characteristics of the voltage and current THD factors and the characteristics of the second harmonics of the current and voltage. The characteristic in Figure 17 clearly shows the increase in power changes ( $P_{\max} - P_{\min}$ ) in successive stages. In stage 1 the variation is approximately 50 W, in stage 2a it increases to approximately 160 W, in stage 2b it decreases to approximately 100 W.



**Figure 17.** The difference between the maximum and minimum active power ( $P_{\max} - P_{\min}$ ) =  $f(t)$  (top), the voltage THD factor  $\text{THDU} = f(t)$ , and current THD factor  $\text{THDI} = f(t)$  (bottom) with the markings of measurement results presented on the waveforms (Figure 21) and amplitude spectra (Figure 20) recorded at 0:05, 1:50, and 2:42 for Case II.

The indicated stages of the charging process are determined by analyzing the nature of active and reactive power. However, as with Case I, stages/sub-stages of the charging process can be determined by analyzing current and voltage harmonics. Figure 17 also shows the characteristics of the current and voltage THD factors. Comparing the characteristics of the current and voltage THD factors, it can be noticed no dependency between changes in the current and voltage distortion (i.e., the increase in the current distortion is not caused by the increase in the voltage distortion). The characteristic of the current THD factor confirms the division of the charging process into two stages. In stage 1, values of the current THD factor are slightly greater than values of the voltage THD factor. In stage 2, values of the current THD factor increase significantly while the voltage THD factor are kept (approximately) constant.

Information about the charging process can be provided by analyzing individual higher harmonics. Considering the properties of the DFT algorithm, even harmonics can be expected in the case of power variation (thus current variations). Figure 18 shows characteristics of the voltage and current THD factors and the characteristics of the second harmonics of the current and voltage.

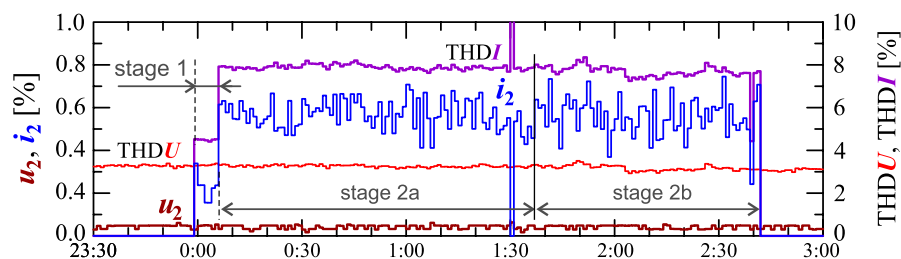


**Figure 18.** The characteristics of the voltage THD factor  $THDU = f(t)$  and current THD factor  $THDI = f(t)$  and the characteristics of the second harmonics of the current  $i_2 = f(t)$  and voltage  $u_2 = f(t)$  for Case II.

As expected, the occurrence of the second harmonic of the current is correlated with the occurrence of the current variation. The characteristic of this harmonic suggests, similar to the characteristic of the current THD factor, the division of the charging process into two stages. Comparing Figure 18 with Figures 16 and 17, it can be seen that the increase in active power changes is associated with an increase in the second harmonic of the current. However, based on Figure 17, it is difficult to determine the sub-stages (stage 2a and stage 2b) in stage 2. In order to obtain information about these sub-stages, the occurrence of higher harmonics of the current should be analyzed. The characteristics of odd harmonics of the current  $i_h$  from the order  $h = 3$  to 13 are shown in Figure 19.

Analyzing characteristics  $i_h = f(t)$  in Figure 19 for harmonics  $h = 3, 5, 9, 11,$  and  $13$ , stages 1 and 2 can be easily identified. Determination of sub-stages in stage 2 is possible only on the basis of the nature of the 7th harmonic of the current. In stage 2a, the 3rd and 7th harmonic values are close, and in stage 2b, the 7th harmonic value is noticeably different compared to the 3rd harmonic. The increase in the contribution of the odd harmonics in stage 2 is probably related to the operation of the power electronic converter in the charging system, causing harmonics of the order of  $6n \pm 1$ , where  $n$  is any natural number. The tendency in the nature of harmonics  $h > 13$  is analogous to Case I; therefore, the presentation of characteristics of these harmonics is omitted. Analyzing characteristics of the current THD factor in Figures 17 and 18 and the characteristics of higher harmonics  $i_h = f(t)$  in Figure 19, an increase in current distortion can be seen.

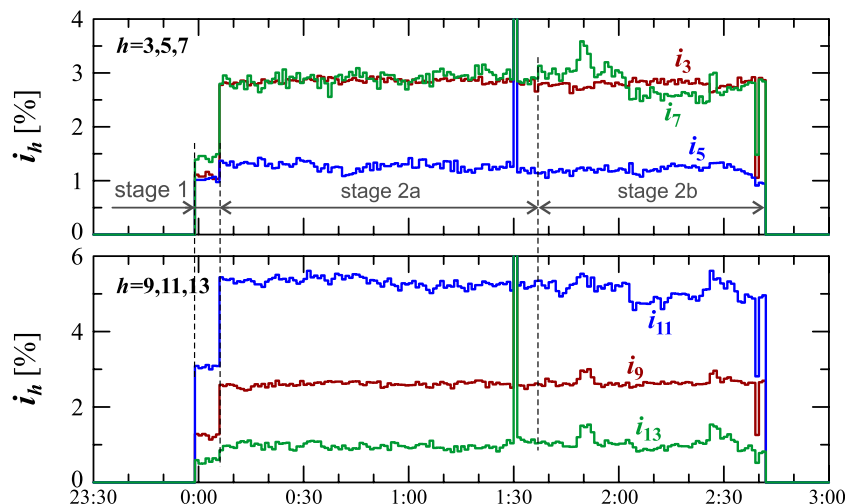


**Figure 19.** The characteristics of odd harmonics of the current  $i_h = f(t)$  from the order  $h = 3$  to 13 for Case II.

Figure 20 shows the amplitude spectrum of the current recorded at 00:05, 1:50, and 2:42 (recording times are marked in Figure 17). Recreated current waveforms on the basis of the recorded harmonics are shown in Figure 21.

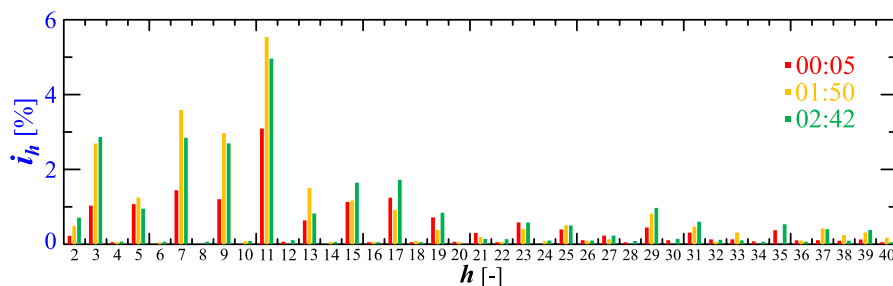


Figure 20. The amplitude spectrum of the current  $i_h = f(h)$  recorded at 00:05, 1:50, and 2:42 for Case II.

Figures 20–23 confirm the non-stationarity of the charging process characterized by the changes in the current waveform and, thus, the changes in the contribution of individual harmonic values in successive time steps. Based on waveforms presented in Figures 21 and 23, conclusions can also be made with regard to the requirements of measuring equipment used to measure selected quantities when charging an electric vehicle. Namely, it is worth noting that the current waveform is strongly non-stationary, and as a consequence, it can lead to significant errors in the measurement of higher harmonics, considering the requirements of the currently used power quality analyzers. Minimizing errors in determining harmonics for waveforms whose nature is similar to the current consumed by the EV onboard charger requires a preliminary algorithm for effective detection of quasi-fundamental periods. Such a procedure also ensures the minimization of errors in determining other parameters for periodic signals.

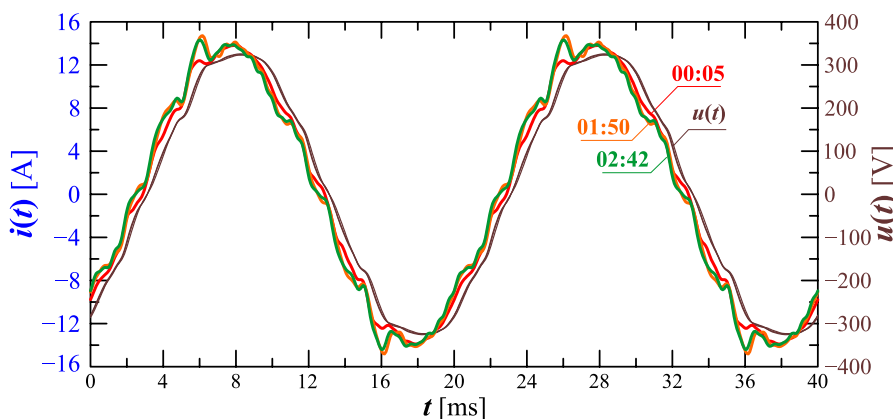


Figure 21. Recreated voltage waveforms  $u(t)$  and current waveforms  $i(t)$  recorded at 00:05, 1:50, and 2:42 for Case II.

Figures 22 and 23 show the amplitude spectrum and recreated current waveforms at 1:30, 1:31, and 1:32.

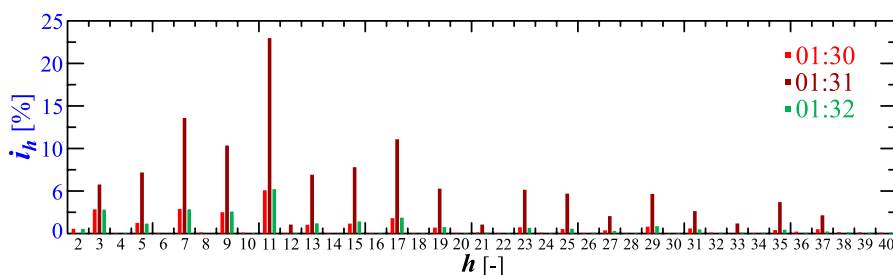
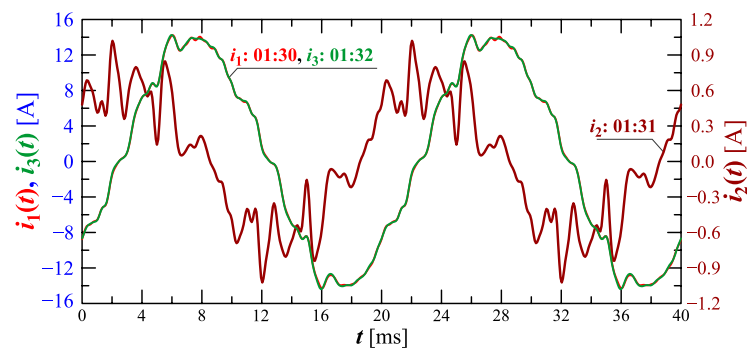


Figure 22. The amplitude spectrum of the current  $i_h = f(h)$  recorded at 01:30, 01:31, and 01:32 for Case II.



**Figure 23.** Recreated voltage waveforms  $u(t)$  and current waveforms  $i(t)$  recorded at 01:30, 01:31, and 01:32 for Case II.

### 3.3. Other Cases

Cases III–V are presented in one subsection because the trends in changes in the rms value,  $P_{st}$  indicator, higher harmonics with order greater than the 13th order, or changes in waveforms of the current consumed by the EV onboard charger are similar to Case I and Case II. Characteristics of changes in the active power, reactive power, voltage, and current THD factors, and harmonics up to the 13th order are presented below because they allow indicating a slightly different nature of the phenomenon occurring during the monitored charging process of an electric vehicle.

Figures 24–28 show the measurement results during the charging process defined as Case III. Two dominant stages: 1 and 2 (main charging phase) and two additional stages: 3 and 4 (additional charging phase) can be indicated on the basis of changes in reactive power (Figure 24). Two sub-stages (stage 2a and stage 2b) can be determined in stage 2. Figure 24 also shows the characteristics of maximum  $I_{max} = f(t)$  and minimum  $I_{min} = f(t)$  values of rms values of the current. Figure 25 shows characteristics of maximum  $P_{max}$ , average  $P_{avg}$  and minimum  $P_{min}$  of active power, on a properly scaled characteristic, in relation to the characteristics of maximum  $U_{max}$  and minimum  $U_{min}$  rms values of the voltage, to better highlight active power changes during charging of an electric vehicle. In stages 1, 2a, and 2b, there is a trend of linear increase in the active power consumed with distinct step changes in the active power value. The characteristic of average values of active power has a shape similar to the sawtooth signal. Quasi-linear power increases can be explained by charging the battery pack in constant current mode. The characteristic  $(P_{max} - P_{min}) = f(t)$  in Figure 26 shows that during the tested charging process, the active power often changes. In stage 1, the active power changes are between 25 W and 75 W. In stage 2a, the active power changes are between 50 W and 125 W. In stage 2b, the active power changes are over 150 W. In stage 3, the active power changes are associated with both stage 1 and stage 2. Comparing the values of active and reactive power (of a capacitive nature) in stage 4 (Figure 24) and active power changes 26 in stage 4, it can be assumed that the charging system in stage 4 is in standby mode (until the charging circuit plug is disconnected). In this mode, there is reactive power associated with the charging of capacitors at the inputs of converter systems. Figure 26 also shows the characteristics of the current and voltage THD factors. Comparing the characteristics of the current and voltage THD factors, unlike Case I and II, it can be seen a certain relationship between the current and voltage distortion in stage 2b of the main charging phase and stage 3 of the additional charging phase—the increase in current distortion is correlated with the increase in voltage distortion. In other stages/sub-stages, there is no relationship between the voltage and current THD values. Considering no dependency between the THD factor of the current and voltage in other stages (including other cases) and the fact that the battery pack charging system is supplied at a close distance to the MV/LV transformer (low impedance of the power supply circuit), it can be concluded that the THD factor of the voltage noticeably affects the THD factor of the current. Thus, the deterioration of the voltage quality amplifies the deterioration of the current consumed by the charger

system. The characteristic of the current THD factor in Figure 26 confirms the division of the charging process into stages proposed on the basis of characteristics of active and reactive power (Figures 24 and 25). Figure 27 shows characteristics of the voltage and current THD factors and the characteristics of the second harmonics of the current and voltage. The characteristic of the second harmonic of the current suggests the division of the charging process into three stages, from 1 to 3, omitting stage 4. Analyzing the characteristics of odd harmonics in Figure 28, different characters of individual harmonics than in Cases I and II can be noticed. Each of the higher harmonic characteristics suggests the division of the charging process into three stages (similar to the active power characteristics in Figures 24–26). In stage 1, higher harmonic steps change their values to specific levels (with low variations). Between stage 1 and stage 2, there is a next step change in the harmonic values. In stage 2, the characteristic of the 3rd harmonic has a downward tendency, and the characteristics of other harmonics have an upward tendency. The 7th and 11th harmonics indicate the determination of two sub-stages (stage 2a and stage 2b) in stage 2.

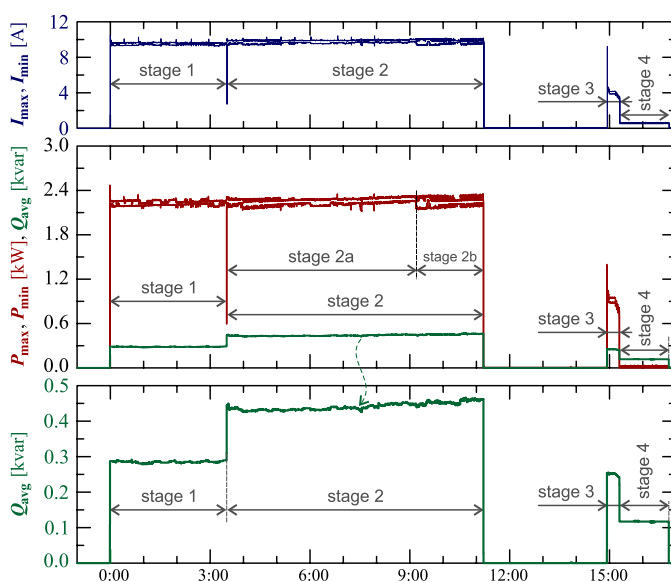


**Figure 24.** The characteristics of maximum  $P_{max} = f(t)$  and minimum  $P_{min} = f(t)$  values of active power and average values of reactive power  $Q_{avg} = f(t)$  for Case III.

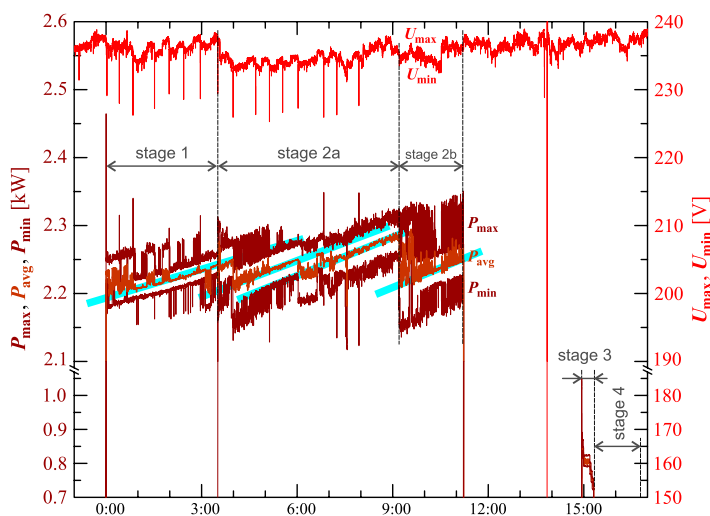


**Figure 25.** The characteristic of maximum  $P_{max} = f(t)$ , average  $P_{avg} = f(t)$  and minimum  $P_{min} = f(t)$  values of active power and maximum  $U_{max} = f(t)$  and minimum  $U_{min} = f(t)$  rms values of supply voltage for Case III; cyan lines are added in the background to indicate the quasi-linear increase in average values of active power.

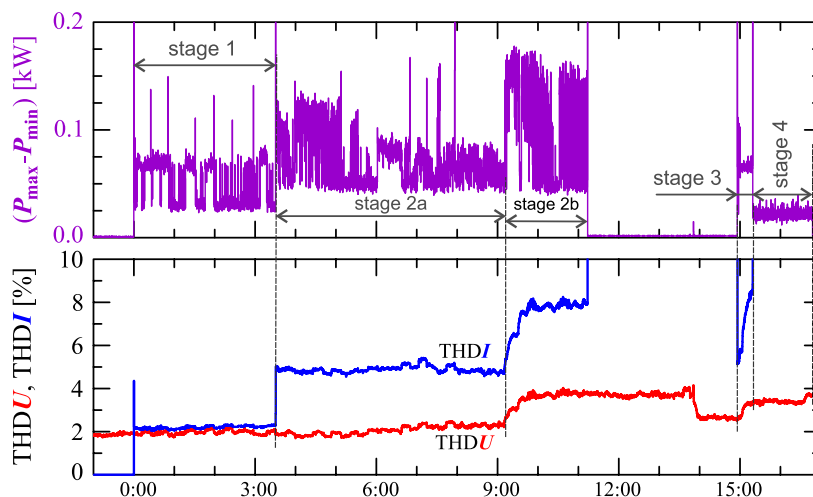


**Figure 26.** The characteristic of difference between the maximum and minimum active power ( $P_{\max} - P_{\min} = f(t)$ ) (top), and the characteristics of the voltage THD factor  $THDU = f(t)$  and current THD factor  $THDI = f(t)$  (bottom) for Case III.

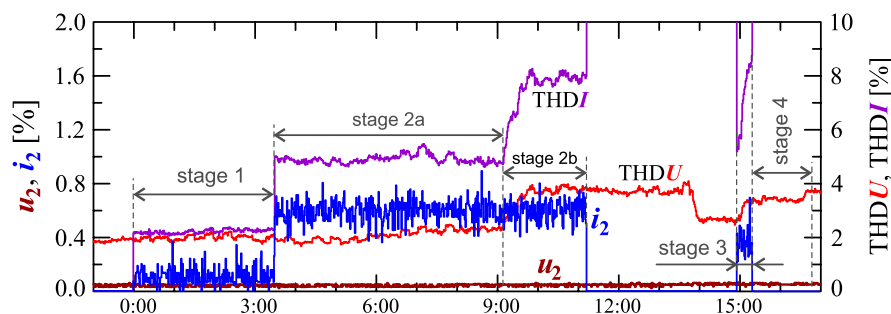


**Figure 27.** The characteristics of the voltage THD factor  $THDU = f(t)$  and current THD factor  $THDI = f(t)$  and the characteristics of the second harmonics of the current  $i_2 = f(t)$  and voltage  $u_2 = f(t)$  for Case III.

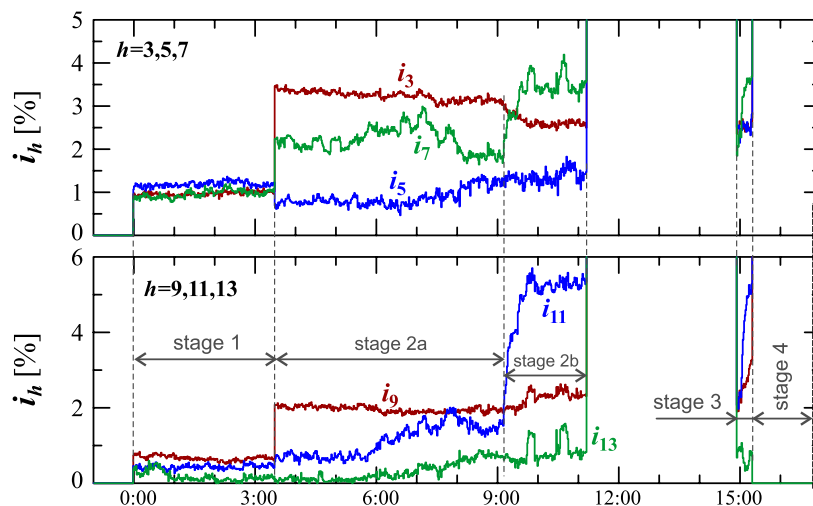


**Figure 28.** The characteristics of odd harmonics of the current  $i_h = f(t)$  from the order  $h = 3$  to 13 for Case III.

Figures 29–33 show the measurement results during the charging process defined as Case IV. Characteristics of active and reactive power (Figure 29) show the main charging phase (stage 1), and two additional charging phases (stages 2–4). The first additional charging phase consists of two stages (stages 2–3), and stage 4 is the second additional charging phase. Stage 3 is the standby mode of the charging system (like stage 3 for

Case III). Stages 2 and 4 are short-term supplementary charging with active and reactive power changes similar to stage 1 (Figure 31). However, for stages 2 and 4, the current distortion is significantly higher than for stage 1 (Figures 31–33). This is especially visible for the 3rd and 5th harmonics. In Figure 30, it can be seen that the increase in values of the voltage THD factor is related to the increase in values of the current THD factor associated with the increase in 11th and 7th harmonics (Figures 31 and 33).

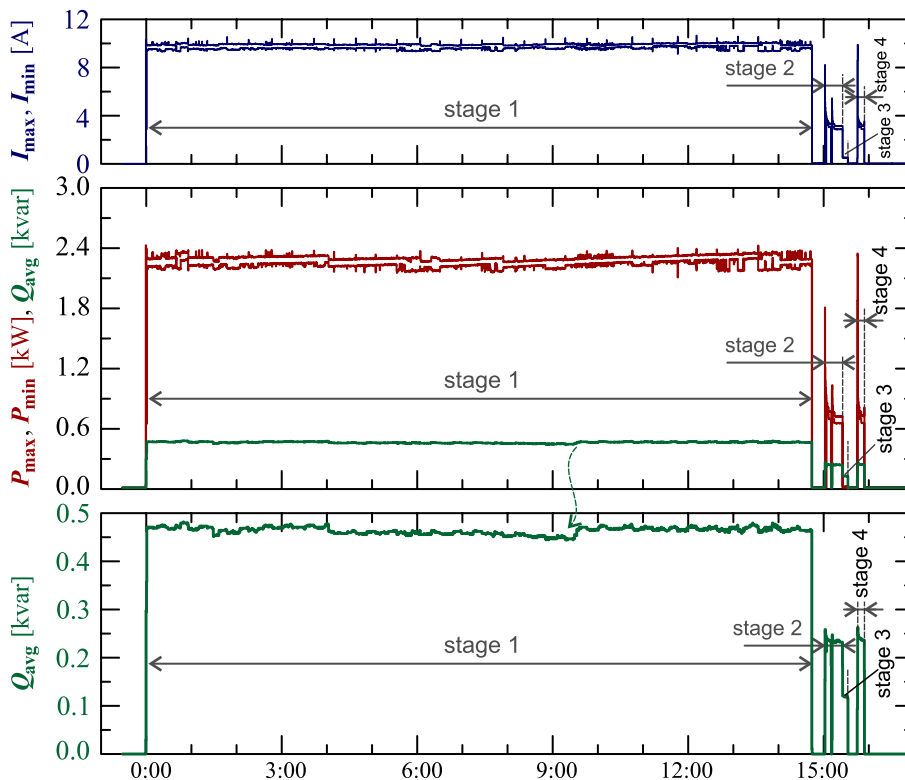


Figure 29. The characteristics of maximum  $P_{max} = f(t)$  and minimum  $P_{min} = f(t)$  values of active power and average values of reactive power  $Q_{avg} = f(t)$  for Case IV.

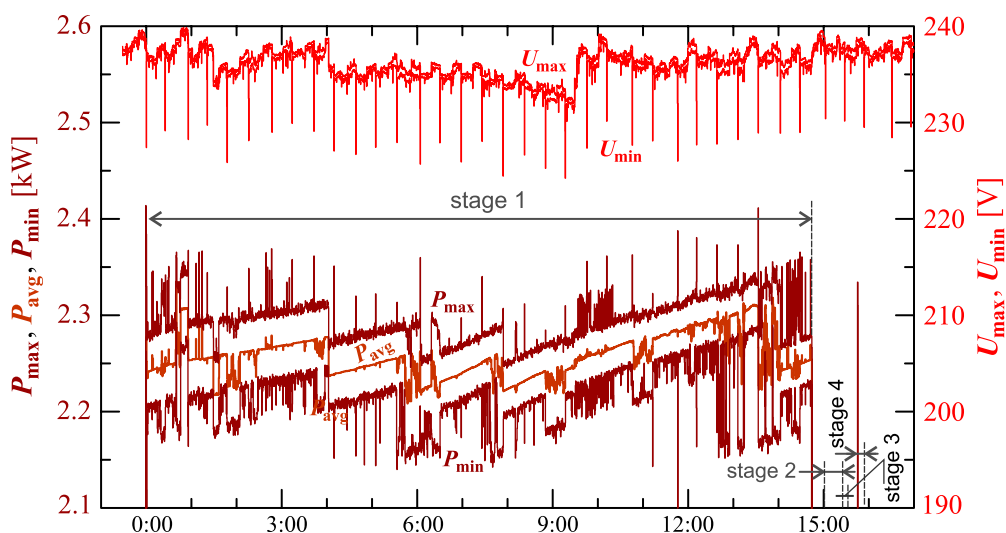
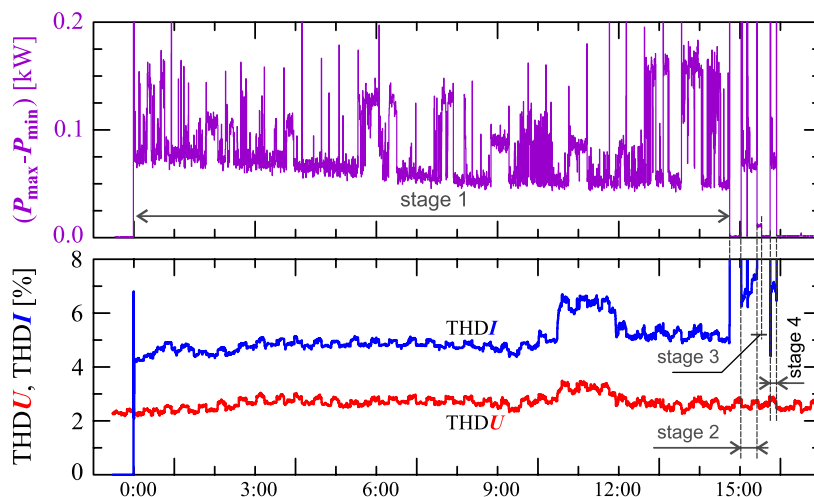
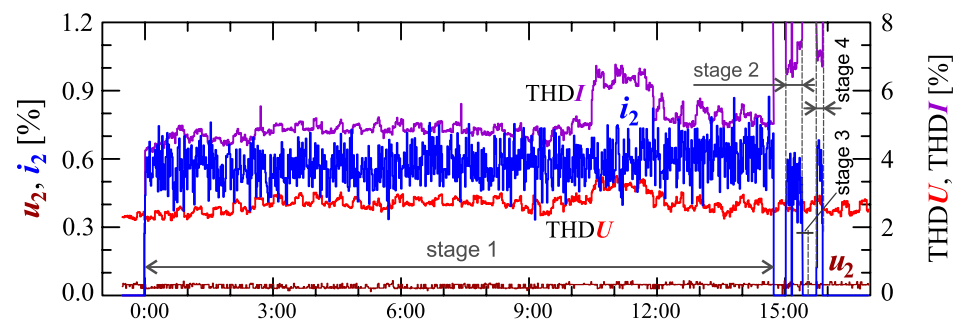


Figure 30. The characteristic of maximum  $P_{max} = f(t)$ , average  $P_{avg} = f(t)$  and minimum  $P_{min} = f(t)$  values of active power and maximum  $U_{max} = f(t)$  and minimum  $U_{min} = f(t)$  rms values of supply voltage for Case IV.



**Figure 31.** The characteristic of difference between the maximum and minimum active power ( $P_{\max} - P_{\min} = f(t)$ ) (top), and the characteristic of the voltage THD factor  $THDU = f(t)$  and current THD factor  $THDI = f(t)$  (bottom) for Case IV.



**Figure 32.** The characteristics of the voltage THD factor  $THDU = f(t)$  and current THD factor  $THDI = f(t)$  and the characteristics of the second harmonics of the current  $i_2 = f(t)$  and voltage  $u_2 = f(t)$  for Case IV.

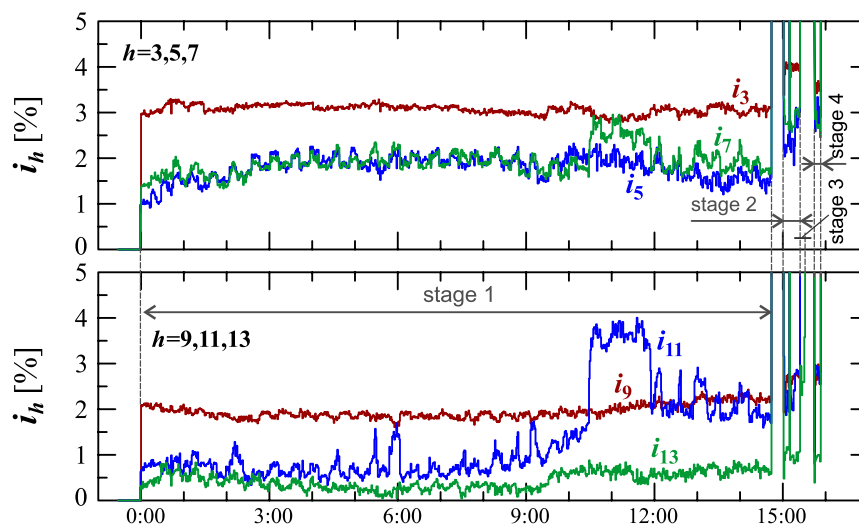


**Figure 33.** The characteristics of odd harmonics of the current  $i_h = f(t)$  from the order  $h = 3$  to 13 for Case IV.

Figures 34–38 show results of measurements for the longest charging process among those presented, defined as Case V. The characteristic of reactive power in Figure 34 shows

that the charging process consists of 3 stages. Based on Figures 34 and 35, it can be concluded that the smallest active power changes occur in stages 1 and 3. Analyzing characteristics of active power, stage 2 can be divided into different sub-stages. For the purpose of the charging process analysis, a division into 3 sub-stages: 2a, 2b, and 2c, is adopted. Stage 2b has the highest changes in the active power. Stages 2a and 2c have comparable active power changes. In stage 2c there is a greater current distortion than in stage 2a. The increase in the value of the THD factor in stage 2c (Figure 38) results from the increase in harmonics from  $h = 7$  to 13 with a simultaneous decrease in the 3rd and 5th harmonics. It is worth noting that stages 1 and 3, despite the similarity of characteristics of active and reactive power, stages differ in current distortion. This can be due to the increase in the value of the voltage THD factor in stage 3 relative to stage 1, with the influence of the THD values on the individual harmonics of the current being different.

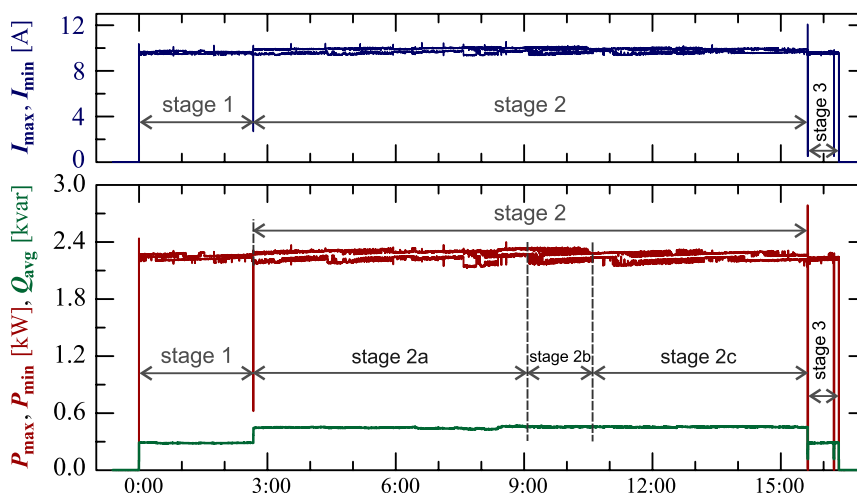


**Figure 34.** The characteristics of maximum  $P_{max} = f(t)$  and minimum  $P_{min} = f(t)$  values of active power and average values of reactive power  $Q_{avg} = f(t)$  for Case V.

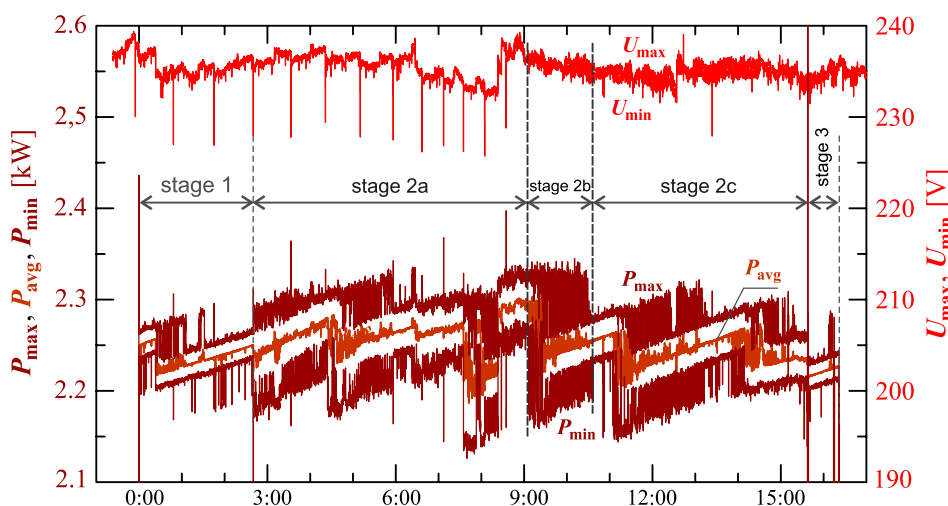


**Figure 35.** The characteristic of maximum  $P_{max} = f(t)$ , average  $P_{avg} = f(t)$  and minimum  $P_{min} = f(t)$  values of active power and maximum  $U_{max} = f(t)$  and minimum  $U_{min} = f(t)$  rms values of supply voltage for Case V.

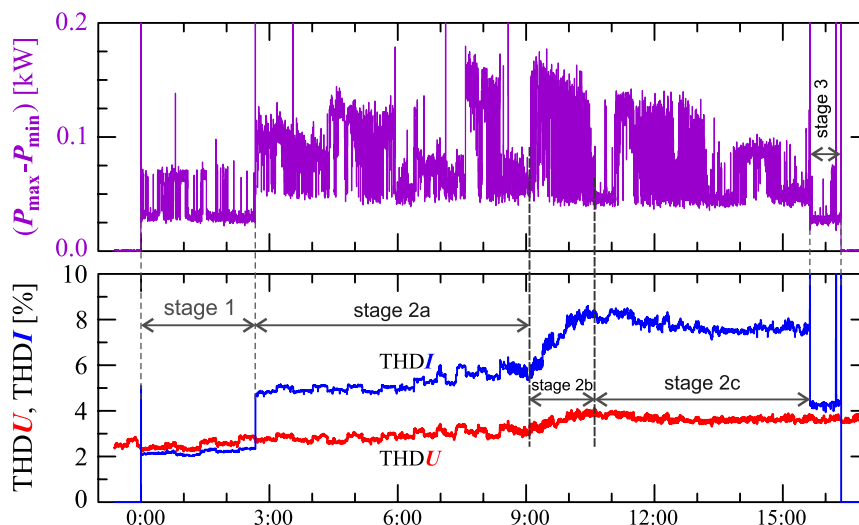


**Figure 36.** The characteristic of difference between the maximum and minimum active power  $(P_{\max} - P_{\min}) = f(t)$  (top), and the characteristic of the voltage THD factor  $THDU = f(t)$  and current THD factor  $THDI = f(t)$  (bottom) for Case V.

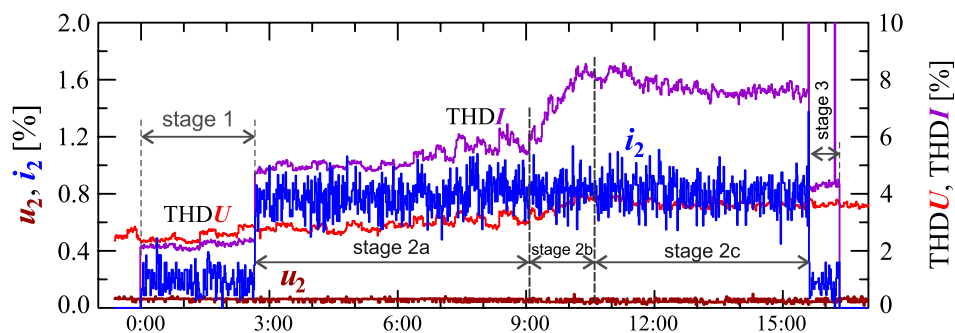


**Figure 37.** The characteristics of the voltage THD factor  $THDU = f(t)$  and current THD factor  $THDI = f(t)$  and the characteristics of the second harmonics of the current  $i_2 = f(t)$  and voltage  $u_2 = f(t)$  for Case V.

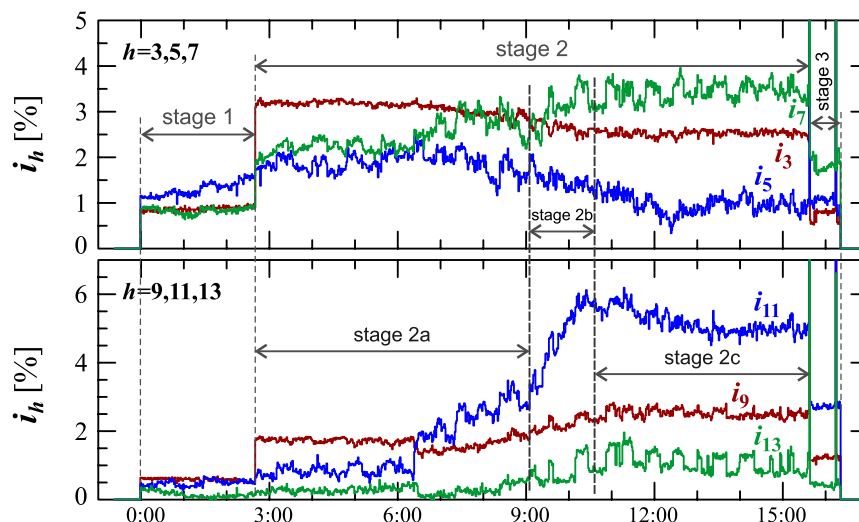


**Figure 38.** The characteristics of odd harmonics of the current  $i_h = f(t)$  from the order  $h = 3$  to 13 for Case V.

In the presented charging processes (Figures 5, 15, 25, 30 and 35) characteristic of average values of active power is similar to the sawtooth signal. Analyzing indicated characteristics, it can be seen that the slope of individual teeth of the sawtooth signal

is different. Figure 39 shows the characteristic of average values of active power for Case V with information about the slope in graphical (trend lines) and numerical (value in W/h) form.

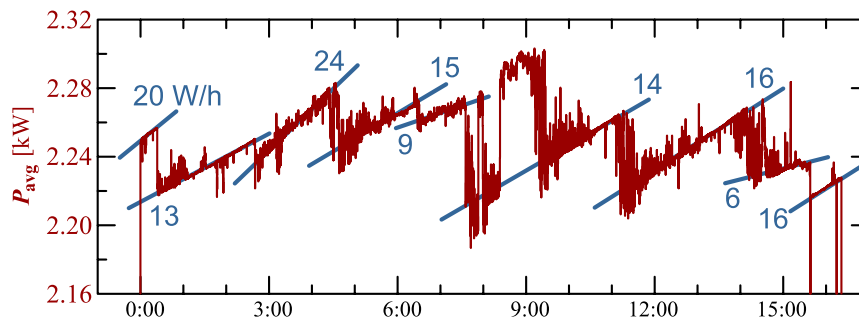


**Figure 39.** The characteristic of the average values of active power for Case V with information about the slope in graphical (trend lines) and numerical (value in W/h) form.

The characteristic of average values of active power indicates that charging is a complex and non-monotonic process. This allows for the conclusion that the charging process is characterized by a high variation of average and instantaneous values of active power.

Analyzing the charging processes referred to as Cases I–V, it is worth noting the relationship between the individual voltage and current harmonics. Figure 40 shows the calculated correlation  $r$  values of the  $h$ -th harmonics of the voltage and current for Cases I–V. Pearson’s linear correlation  $r$  coefficient is calculated according to the relation:

$$r = \frac{\sum_{i=1}^N (x_i - \bar{x})(y_i - \bar{y})}{\sqrt{\sum_{i=1}^N (x_i - \bar{x})^2} \sqrt{\sum_{i=1}^N (y_i - \bar{y})^2}}, \tag{1}$$

where  $x$  and  $y$  are the considered measurement series included in the statistical analysis (e.g., selected  $h$ -th harmonic of the voltage and current over time),  $\bar{x}$  and  $\bar{y}$  are the calculated values of the arithmetic mean for the series marked as  $x$  and  $y$ , respectively.

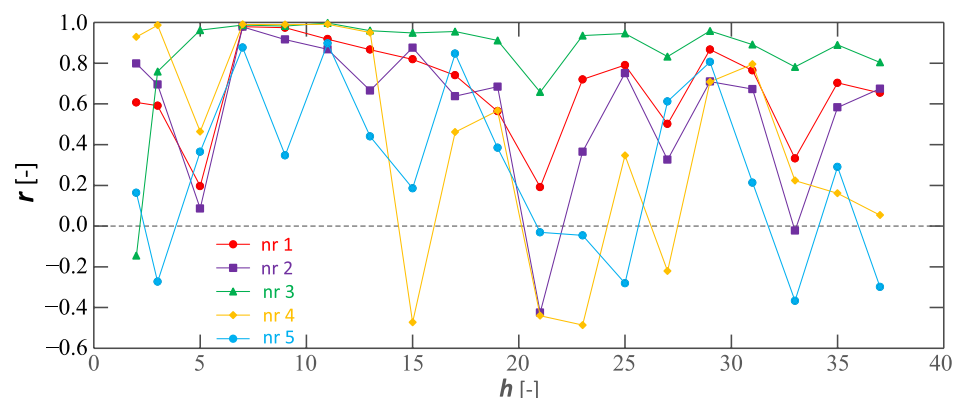


**Figure 40.** Correlation  $r$  coefficient of characteristics of  $h$ -th harmonics of the voltage and current for considered charging processes, which are defined as Cases I–V.

Analyzing characteristics shown in Figure 40, it can be seen that for some voltage and current harmonics, in particular for  $h = 7, 11,$  and  $29$ , a strong statistical relationship is visible. When considering the relationships between individual harmonics, it is worth noting that the EV onboard charger is supplied by a low-impedance line. In this case, the effect of the current distortion should not significantly affect the voltage distortion, i.e., a strong statistical relationship between voltage and current is not expected. This is consistent with the observations of Cases I–V. The cases in which there is a strong statistical relationship for specific harmonics are difficult to explain. Perhaps this is the result of the

occurrence of states close to parallel resonance, for which small values of the current can cause significant values of the voltage. Detection of such states is problematic, especially since the properties of the power supply circuit can change in real-time (connection and disconnection of different loads, including those of a resistive–capacitive nature).

The results of monitoring the selected cases presented in the paper show the non-stationarity of the phenomena occurring during the charging of an electric vehicle. The onboard charger is a power electronics system. Therefore, it is difficult to determine the impact of such a system on power quality during charging. This results in the postulate of supervision of the charging process, especially at the beginning of EV use. It should be emphasized that the effects of EV onboard charger operation can be amplified with an increasing impedance of the power supply circuit. Determination of the impact of charging on power quality requires considering the possible operation of other EV onboard chargers, e.g., at a neighbor connected to the same LV line.

#### 4. Conclusions

The paper presents the results of the monitoring of the process of charging an electric vehicle battery pack in a single-phase 230 V/50 Hz circuit. This process is managed by the EV onboard charger. In the monitoring process, the focus is on the recognition of the charging process, considering the impact of this process on the power quality and consequently on the reliability of electric machines. The research results indicate that the monitored processes of the charging of an electric vehicle are non-stationary, and are characterized, for example, by different numbers of stages/sub-stages, within which individual parameters assume specific values. The individual stages/sub-stages are characterized by variations of the currents, active and reactive power, and higher harmonic contributions. The observed changes have different causes. The quasi-linear slow increase of active power is related to the increase of the voltage on the battery pack during charging. Other types of changes, which have short-term phenomena, are associated with the operation of an EV onboard charger. In particular, the operation of the PFC system can cause changes in the current and power. The operation of the EV onboard charger depends on the control algorithm implemented in it. If EV onboard chargers have compatible topologies, it can be expected that the variation of powers (active and reactive) and parameters assessing power quality can be similar. However, for different topologies, it is advisable to carry out the research presented in the paper. The effects of current, active, and reactive power and higher harmonics changes depend on the characteristics of the power grid at the point of connection of the charging system. The effects of such changes can be amplified if the vehicle's charging system is supplied by a high-impedance line. Knowledge of the voltage, current, and power variation allows for the specification of requirements for the measurement equipment used to monitor the charging process, including the determination of the discrimination/averaging time of the monitored quantities. The obtained research results indicate the need for continuous monitoring of power quality in the particular circuit, where electrical loads (e.g., electric machines) are supplied. Continuous monitoring supports the diagnosis of electrical machines and allows for appropriate actions to increase their reliability.

**Author Contributions:** Conceptualization, P.K. and G.W.; methodology, P.K. and G.W.; software, G.W.; validation, P.K. and G.W.; formal analysis, P.K. and G.W.; resources, P.K. and G.W.; data curation, P.K. and G.W.; writing—original draft preparation, P.K. and G.W.; visualization, P.K. and G.W.; supervision, P.K. and G.W.; project administration, G.W.; funding acquisition, P.K. All authors have read and agreed to the published version of the manuscript.

**Funding:** This research was partially supported by the Ministry of Education and Science under Grant number 0212/SBAD/0569.

**Institutional Review Board Statement:** Not applicable.

**Informed Consent Statement:** Not applicable.

**Data Availability Statement:** Not applicable.

**Conflicts of Interest:** The authors declare no conflict of interest.

## References

1. 6th CEER Benchmarking Report on All the Quality of Electricity and Gas Supply 2016. 2016. Available online: <https://www.ceer.eu/> (accessed on 1 September 2021).
2. Mozaffari, M.; Doshi, K.; Yilmaz, Y.C. Real-Time Detection and Classification of Power Quality Disturbances. *Sensors* **2022**, *22*, 7958. [[CrossRef](#)] [[PubMed](#)]
3. Valtierra-Rodriguez, M.; Rivera-Guillen, J.R.; Basurto-Hurtado, J.A.; De-Santiago-Perez, J.J.; Granados-Lieberman, D.; Amezcua-Sanchez, J.P.C. Convolutional Neural Network and Motor Current Signature Analysis during the Transient State for Detection of Broken Rotor Bars in Induction Motors. *Sensors* **2020**, *20*, 3721. [[CrossRef](#)]
4. Gnacinski, P.; Mindykowski, J.; Tarasiuk, T. Effect of power quality on windings temperature of marine induction motors. Part II: Results of investigations and recommendations for related regulations. *Energy Convers. Manag.* **2009**, *50*, 2477–2485. [[CrossRef](#)]
5. Gnacinski, P.; Peplinski, M.; Murawski, L.; Szelezinski, A. Vibration of Induction Machine Supplied With Voltage Containing Subharmonics and Interharmonics. *IEEE Trans. Energy Convers.* **2019**, *34*, 1928–1937. [[CrossRef](#)]
6. Holopainen, T.P.; Jorg, P.; Niiranen, J.; Andrea, D. Electric Motors and Drives in Torsional Vibration Analysis and Design. In Proceedings of the 42nd Turbomachinery Symposium, College Station, TX, USA, 1–3 October 2013.
7. Gonzalez-Abreu, A.D.; Osornio-Rios, R.A.; Jaen-Cuellar, A.Y.; Delgado-Prieto, M.; Antonino-Daviu, J.A.; Karlis, A. Advances in Power Quality Analysis Techniques for Electrical Machines and Drives: A Review. *Energies* **2022**, *15*, 1909. [[CrossRef](#)]
8. Fuchs, E.; Masoum, M. *Power Quality in Power Systems, Electrical Machines, and Power-Electronic Drives*, 3rd ed.; Academic Press: Cambridge, MA, USA, 2022.
9. Ferreira, F.J.T.E.; Baoming, G.; de Almeida, A.T. Reliability and operation of high-efficiency induction motors. In Proceedings of the 2015 IEEE/IAS 51st Industrial & Commercial Power Systems Technical Conference (I&CPS), Calgary, AB, Canada, 5–8 May 2015; pp. 1–13. [[CrossRef](#)]
10. Donolo, P.D.; Pezzani, C.M.; Bossio, G.R.; De Angelo, C.H.; Donolo, M.A. Derating of Induction Motors Due to Power Quality Issues Considering the Motor Efficiency Class. *IEEE Trans. Ind. Appl.* **2020**, *56*, 961–969. [[CrossRef](#)]
11. Gnacinski, P.; Hallmann, D.; Peplinski, M.; Jankowski, P. The effects of voltage subharmonics on cage induction machine. *Int. J. Electr. Powe Energy Syst.* **2019**, *111*, 125–131. [[CrossRef](#)]
12. Gnacinski, P.; Hallmann, D.; Muc, A.; Klimczak, P.; Peplinski, M. Induction Motor Supplied with Voltage Containing Symmetrical Subharmonics and Interharmonics. *Energies* **2022**, *15*, 7712. [[CrossRef](#)]
13. Chauhan, S.; Singh, S.B. Effects of Voltage Unbalance and Harmonics on 3-Phase Induction Motor During the Condition of Undervoltage and Overvoltage. In Proceedings of the 2019 6th International Conference on Signal Processing and Integrated Networks (SPIN), Noida, India, 7–8 March 2019; pp. 1141–1146. [[CrossRef](#)]
14. Gnacinski, P.; Hallmann, D.; Klimczak, P.; Muc, A.; Peplinski, M. Effects of Voltage Interharmonics on Cage Induction Motors. *Energies* **2021**, *14*, 1218. [[CrossRef](#)]
15. Kini, G.P.; Bansal, R.C.; Aithal, R.S. Impact of voltage unbalance on the performance of three-phase induction motor. *S. Pac. J. Nat. Sci.* **2006**, *24*, 45–50 [[CrossRef](#)]
16. Gumilar, L.; Afandi, A.N.; Sujito; Faiz, M.R. Starting Induction Motor at Different Voltage Levels in the Electrical Power System. In Proceedings of the 2021 International Conference on Electrical and Information Technology (IEIT), Malang, Indonesia, 14–15 September 2021; pp. 269–273. [[CrossRef](#)]
17. Sousa, V.; Hernandez, H.; Quispe, E.C.; Gomez, J.R.; Viego, P.R. Analysis of harmonic distortion generated by PWM motor drives. In Proceedings of the 2017 IEEE Workshop on Power Electronics and Power Quality Applications (PEPQA), Bogota, Colombia, 31 May–2 June 2017; pp. 1–6. [[CrossRef](#)]
18. Masoum, M.; Fuchs, E. *Power Quality in Power Systems, Electrical Machines, and Power-Electronic Drives*, 2nd ed.; Academic Press: Cambridge, MA, USA, 2015.
19. Siostrzonek, T.; Chmielowiec, K.; Firlit, A.; Barcentewicz, S. Advantages and disadvantages of using multi-pulse systems in the electric drive of hoisting machines. *Prz. Elektrotech.* **2020**, *96*, 43–46. [[CrossRef](#)]
20. Langella, R.; Testa, A.; Vendemia, V.; Drapela, J. New Comprehensive Analytical Model of Single-Phase AC/DC Diode Rectifiers in the Presence of Interharmonics in Supply Voltage. In Proceedings of the 2022 20th International Conference on Harmonics and Quality of Power (ICHQP 2022), Naples, Italy, 29 May–1 June 2022. [[CrossRef](#)]
21. Crotti, G.; Chen, Y.; Çayci, H.; D’Avanzo, G.; Landi, C.; Letizia, P.S.; Luiso, M.; Mohns, E.; Muñoz, F.; Styblikova, R.; et al. How Instrument Transformers Influence Power Quality Measurements: A Proposal of Accuracy Verification Tests. *Sensors* **2022**, *22*, 5847. [[CrossRef](#)]
22. Ray, P.K. Power quality improvement using VLLMS based adaptive shunt active filter. *CPSS Trans. Power Electron. Appl.* **2018**, *3*, 154–162. [[CrossRef](#)]
23. Alali, M.A.E.; Shtessel, Y.B.; Barbot, J.P.; Di Gennaro, S. Sensor Effects in LCL-Type Grid-Connected Shunt Active Filters Control Using Higher-Order Sliding Mode Control Techniques. *Sensors* **2022**, *22*. [[CrossRef](#)]
24. Upadhyay, A.; Mahala, H.C. Review of Shunt Active Power Filters for Compensation. *Int. J. Eng. Res. Curr. Trends* **2021**, *3*, 3–4.

25. Adabara, I.C. Design and Implementation of an Automatic High-Performance Voltage Stabilizer. *Int. J. Eng. Inf. Syst.* **2018**, *2*, 1–10.
26. Karimov, R.C.; Kuchkarov, A.V.; Xodjalimova, M.Z.; Makhamadjanov, R.K.; Numonov, A.B. Analysis and study of energy efficiency by the operation of a voltage stabilizer. *J. Phys. Conf. Ser.* **2021**, *2094*, 052050. [\[CrossRef\]](#)
27. Das, S.R.; Ray, P.K.; Mohanty, A. Improvement in Power Quality using Hybrid Power Filters based on RLS Algorithm. *Energy Procedia* **2017**, *138*, 723–728. [\[CrossRef\]](#)
28. Jarupula, S.; Vutlapalli, N.C. Power Quality Improvement in Distribution System using ANN Based Shunt Active Power Filter. *Int. J. Power Electron. Drive Syst.* **2015**, *5*, 568–575. [\[CrossRef\]](#)
29. Wiczynski, G. Diagnostic capabilities of voltage fluctuation indices—A case study. In Proceedings of the 2012 IEEE 15th International Conference on Harmonics and Quality of Power, Hong Kong, China, 17–20 June 2012; pp. 414–419. [\[CrossRef\]](#)
30. Edelstein, S. Study suggests EV drivers are more satisfied with wall chargers vs mobile cords. In *Green Car Reports*; Internet Brands: El Segundo, CA, USA, 2021.
31. Gomez, J.; Morcos, M. Impact of EV battery chargers on the power quality of distribution systems. *IEEE Trans. Power Deliv.* **2003**, *18*, 975–981. [\[CrossRef\]](#)
32. Enslin, J.; Heskes, P. Harmonic interaction between a large number of distributed power inverters and the distribution network. *IEEE Trans. Power Electron.* **2004**, *19*, 1586–1593. [\[CrossRef\]](#)
33. Pankaj, S.; Khalid, M.R.; Saad Alam, M.; Jamil Asghar, M.S.; Hameed, S. Electric Vehicle Charging Stations and their Impact on the Power Quality of Utility Grid. In Proceedings of the 2022 International Conference on Decision Aid Sciences and Applications (DASA), Chiangrai, Thailand, 23–25 March 2022; pp. 816–821. [\[CrossRef\]](#)
34. Karmaker, A.K.; Roy, S.; Ahmed, M.R. Analysis of the Impact of Electric Vehicle Charging Station on Power Quality Issues. In Proceedings of the 2019 International Conference on Electrical, Computer and Communication Engineering (ECCE), Cox’s Bazar, Bangladesh, 7–9 February 2019; pp. 1–6. [\[CrossRef\]](#)
35. Alshareef, S.M.; Morsi, W.G. Impact of fast charging stations on the voltage flicker in the electric power distribution systems. In Proceedings of the 2017 IEEE Electrical Power and Energy Conference (EPEC), Saskatoon, SK, Canada, 22–25 October 2017; pp. 1–6. [\[CrossRef\]](#)
36. Garn, T.; Vanselow, A.; Biedermann, C.; Moser, A.; Engel, B. Flicker emission of electric vehicle charging in low voltage grids. In Proceedings of the CIRED Porto Workshop 2022: E-mobility and Power Distribution Systems, Porto, Portugal, 2–3 June 2022; pp. 294–298. [\[CrossRef\]](#)
37. Alshareef, S.M. Analyzing and Mitigating the Impacts of Integrating Fast-Charging Stations on the Power Quality in Electric Power Distribution Systems. *Sustainability* **2022**, *14*, 5595. [\[CrossRef\]](#)
38. Alshareef, S.M. A Novel Smart Charging Method to Mitigate Voltage Fluctuation at Fast Charging Stations. *Energies* **2022**, *15*, 1746. [\[CrossRef\]](#)
39. Slangen, T.; van Wijk, T.; Cuk, V.; Cobben, S. The Propagation and Interaction of Supraharmonics from Electric Vehicle Chargers in a Low-Voltage Grid. *Energies* **2020**, *13*, 3865. [\[CrossRef\]](#)
40. Meyer, J.; Mueller, S.; Ungethuen, S.; Xiao, X.; Collin, A.; Djokic, S. Harmonic and supraharmonic emission of on-board electric vehicle chargers. In Proceedings of the 2016 IEEE PES Transmission & Distribution Conference and Exposition-Latin America (PES T&D-LA), Michoacán, Mexico, 20–24 September 2016; pp. 1–7. [\[CrossRef\]](#)
41. Yong, J.Y.; Ramachandaramurthy, V.K.; Tan, K.M.; Mithulananthan, N. A review on the state-of-the-art technologies of electric vehicle, its impacts and prospects. *Renew. Sustain. Energy Rev.* **2015**, *49*, 365–385. [\[CrossRef\]](#)
42. Thiringer, T.; Haghbin, S. Power Quality Issues of a Battery Fast Charging Station for a Fully-Electric Public Transport System in Gothenburg City. *Batteries* **2015**, *1*, 22–33. [\[CrossRef\]](#)
43. Jiang, C.; Torquato, R.; Salles, D.; Xu, W. Method to Assess the Power-Quality Impact of Plug-in Electric Vehicles. *IEEE Trans. Power Deliv.* **2014**, *29*, 958–965. [\[CrossRef\]](#)
44. Wang, L.; Qin, Z.; Slangen, T.; Bauer, P.; van Wijk, T. Grid Impact of Electric Vehicle Fast Charging Stations: Trends, Standards, Issues and Mitigation Measures—An Overview. *IEEE Open J. Power Electron.* **2021**, *2*, 56–74. [\[CrossRef\]](#)
45. Ahmed, M.A.; El-Sharkawy, M.R.; Kim, Y.C. Remote Monitoring of Electric Vehicle Charging Stations in Smart Campus Parking Lot. *J. Mod. Power Syst. Clean Energy* **2020**, *8*, 124–132. [\[CrossRef\]](#)
46. Alshahrani, S.; Khalid, M.; Almuahini, M. Electric Vehicles Beyond Energy Storage and Modern Power Networks: Challenges and Applications. *IEEE Access* **2019**, *7*, 99031–99064. [\[CrossRef\]](#)
47. Martinez-Lao, J.; Montoya, F.G.; Montoya, M.G.; Manzano-Agugliaro, F. Electric vehicles in Spain: An overview of charging systems. *Renew. Sustain. Energy Rev.* **2017**, *77*, 970–983. [\[CrossRef\]](#)
48. EN 50160:2010/A2:2019; Voltage Characteristics of Electricity Supplied by Public Electricity Networks. European Committee for Electrotechnical Standardization (CENELEC): Brussels, Belgium, 2019.
49. *Energy Measurements System SPE ENERGO, User Manual*; ZAP MikroTom: Poznań, Poland, 2012.
50. Kyoritsu Electrical Instruments Works, LTD. *Line Up of Clamp Sensors Series, User Manual*; Kyoritsu: Tokyo, Japan, 2006.
51. IEC 61000-4-30:2015/AMD1:2021; Testing and Measurement Techniques—Power Quality Measurement Methods. The International Electrotechnical Commission (IEC): Geneva, Switzerland, 2021.
52. Tao, H.; Zhang, G.; Zheng, Z. Onboard Charging DC/DC Converter of Electric Vehicle Based on Synchronous Rectification and Characteristic Analysis. *Renew. Sustain. Energy Rev.* **2019**, 2613893. [\[CrossRef\]](#)

53. Metwly, M.Y.; Abdel-Majeed, M.S.; Abdel-Khalik, A.S.; Hamdy, R.A.; Hamad, M.S.; Ahmed, S. A Review of Integrated On-Board EV Battery Chargers: Advanced Topologies, Recent Developments and Optimal Selection of FSCW Slot/Pole Combination. *IEEE Access* **2020**, *8*, 85216–85242. [[CrossRef](#)]
54. Xie, F.; Liu, X.; Cui, S.; Li, K. Design of Power Factor Correction System for On-board Charger. In *Intelligent Computing in Smart Grid and Electrical Vehicles*; Li, K., Xue, Y., Cui, S., Niu, Q., Eds.; Springer Berlin Heidelberg: Berlin/Heidelberg, Germany, 2014; 529–538. [[CrossRef](#)]
55. Dewangan, S.K.; Sahu, L.K.; Tiwari, A.K. Single Phase Isolated Onboard Charger for Electric Vehicle. In Proceedings of the 2022 2nd Asian Conference on Innovation in Technology (ASIANCON), Ravet, India, 26–28 August 2022; pp. 1–6. [[CrossRef](#)]
56. Mallik, A.; Lu, J.; Khaligh, A. Sliding Mode Control of Single-Phase Interleaved Totem-Pole PFC for Electric Vehicle Onboard Chargers. *IEEE Trans. Veh. Technol.* **2018**, *67*, 8100–8109. [[CrossRef](#)]
57. Sharma, U.; Singh, B. A Non-isolated Onboard Charger for Electric Vehicle. In Proceedings of the 2021 IEEE Transportation Electrification Conference and Expo (ITEC), Chicago, IL, USA, 21–25 June 2021; pp. 446–451. [[CrossRef](#)]
58. Teng, J.H.; Liao, S.H.; Wen, C.K. Design of a Fully Decentralized Controlled Electric Vehicle Charger for Mitigating Charging Impact on Power Grids. *IEEE Trans. Ind. Appl.* **2017**, *53*, 1497–1505. [[CrossRef](#)]
59. Gupta, J.; Singh, B.; Kushwaha, R. A Rooftop Solar PV Assisted On-Board Enhanced Power Quality Charging System for E-Rickshaw. In Proceedings of the 2020 International Conference on Power, Instrumentation, Control and Computing (PICCC) Online, 28–29 August 2020; pp. 1–6. [[CrossRef](#)]
60. IEC 61000-4-7:2002/A1:2008; Testing and Measurement Techniques—General Guide on Harmonics and Interharmonics Measurements and Instrumentation, for Power Supply Systems and Equipment Connected Thereto. The International Electrotechnical Commission (IEC): Geneva, Switzerland, 2009.
61. Kuwalek, P.; Otomanski, P.; Wandachowicz, K. Influence of the Phenomenon of Spectrum Leakage on the Evaluation Process of Metrological Properties of Power Quality Analyser. *Energies* **2020**, *13*, 5338. [[CrossRef](#)]
62. Carpinelli, G.; Bracale, A.; Varilone, P.; Sikorski, T.; Kostyla, P.; Leonowicz, Z. A New Advanced Method for an Accurate Assessment of Harmonic and Supraharmonic Distortion in Power System Waveforms. *IEEE Access* **2021**, *9*, 88685–88698. [[CrossRef](#)]

**Disclaimer/Publisher’s Note:** The statements, opinions and data contained in all publications are solely those of the individual author(s) and contributor(s) and not of MDPI and/or the editor(s). MDPI and/or the editor(s) disclaim responsibility for any injury to people or property resulting from any ideas, methods, instructions or products referred to in the content.